Clim. Past, 21, 2465–2483, 2025 https://doi.org/10.5194/cp-21-2465-2025 © Author(s) 2025. This work is distributed under the Creative Commons Attribution 4.0 License.





Mid-Holocene sea-ice dynamics and climate in the northeastern Weddell Sea inferred from an Antarctic snow petrel stomach oil deposit

Mark A. Stevenson^{1,a}, Dominic A. Hodgson^{2,1}, Michael J. Bentley¹, Darren R. Gröcke³, Neil Tunstall¹, Chris Longley¹, Alice Graham¹, and Erin L. McClymont¹

Correspondence: Mark A. Stevenson (mark.stevenson@arch.ox.ac.uk)

Received: 3 February 2025 – Discussion started: 25 February 2025

Revised: 16 October 2025 – Accepted: 29 October 2025 – Published: 26 November 2025

Abstract. Understanding past variability in Antarctic sea ice is of critical importance to determine how it regulates global climate processes, biogeochemistry, and Southern Ocean marine ecosystems. Records of changes in Holocene sea-ice conditions in the Weddell Sea are limited to a few marine sediment cores and inferences from continental ice cores. Here we present a novel record of sea ice and climate from \sim 6390 to 1830 cal. yr BP based on accumulation rates and multi-proxy geochemical analyses of a snow petrel stomachoil deposit from the Heimefrontfjella Range, Dronning Maud Land, East Antarctica. Three different sea-ice configurations are interpreted from the record. In the first interval, from 6390 to 5960 cal. yr BP, we see evidence of high productivity and inputs of krill, which suggests foraging both at the continental shelf edge in the marginal ice zone (MIZ) and extending offshore over pelagic waters. We infer that the MIZ lay within the foraging range of Heimefrontfjella. In the second interval, from 5960 to 4320 cal. yr BP, productivity remained high, but there was a reduced influence of krill and likely more fish in the diet. This is consistent with foraging both over the continental shelf edge and offshore, supportive of the summer sea ice retreat reaching the shelf edge more frequently. Finally, in the final interval, between 4320 to 1830 cal. yr BP we infer very low productivity where increased sea-ice conditions restricted access to foraging grounds and open waters, with a less accessible MIZ resulting in a more dense sea-ice pack. Our results highlight how specific Holocene sea-ice configurations can be interpreted from the geochemical composition of snow petrel stomach-oil deposits. We also show, for the first time, the utility of phytol and cholesterol analysis for tracking past avian diet.

1 Introduction

Antarctic sea-ice conditions are highly variable and closely coupled with continental, oceanic and atmospheric processes which both interact with and influence global climate (Brandon et al., 2010). Mechanistically, the formation of sea ice results in brine rejection which can directly contribute to the formation of Antarctic Bottom Water (AABW) (Crosta et al., 2022), helping drive ocean circulation, including the deep overturning cells (Ferrari et al., 2014) and supporting important circulation systems such as the Weddell Gyre (Vernet et al., 2019). Within the sea ice, upwelling can result in the formation of open ocean polynyas (areas of open water), whereas near the coast or at ice shelf fronts polynyas can form as a result of katabatic winds (Comiso and Gordon, 1987). These polynyas can support high levels of primary productivity in the ocean (Smith et al., 2010; Sarmiento et al., 2004; Arrigo et al., 2003).

¹Department of Geography, Durham University, Durham, DH1 3LE, United Kingdom

²British Antarctic Survey, Natural Environment Research Council, Cambridge, CB3 0ET, United Kingdom

³Department of Earth Science, Durham University, Durham, DH1 3LE, United Kingdom

^apresent address: Oxford Radiocarbon Accelerator Unit (ORAU), School of Archaeology, University of Oxford, Dyson Perrins Building, South Parks Road, Oxford OX1 3QY, United Kingdom

Antarctic sea-ice records reveal pronounced declines in extent since 2016, associated with recent warming (Eayrs et al., 2021), with historic lows in 2023 and 2024 (Ionita, 2024; Purich and Doddridge, 2023; Gilbert and Holmes, 2024; National Snow and Ice Data Center (NSIDC), 2024; Wang et al., 2024) and projections of up to 67% decline by 2100 (Collins et al., 2013). Improved palaeoenvironmental reconstructions of Antarctic sea ice are vital to put these instrumental observations (< 50 years) into a longer-term context. Such reconstructions provide a historical basis to understand the interactions between climate and sea-ice conditions, and interactions between sea ice and the extent of floating ice shelves and grounded ice.

Existing knowledge of Holocene Antarctic sea-ice evolution suggests there were three distinct phases, but these can be out of phase geographically due to regional responses and uncertainty associated with dating (Crosta et al., 2022). For coastal records, a cooler early Holocene between 11.5 to 8 ka BP (e.g. Barbara et al., 2010; Denis et al., 2010; Peck et al., 2015; Mezgec et al., 2017; Nichols et al., 2019), was followed by a warmer mid-Holocene (~ 7 to $\sim 4-3$ ka BP) with higher sea surface temperatures and longer ice-free summers (Crosta et al., 2022) and then a cooler late Holocene or "neoglacial" phase $\sim 5-3$ to 1-0 ka BP marked by increased sea-ice extent as surface water temperatures reduced (Barbara et al., 2016; Taylor et al., 2001). However, records retrieved from beyond the coastal regions or those influenced by CDW (Circumpolar Deep Water) show an opposite pattern, with a warmer late Holocene (Bianchi and Gersonde, 2004; Nielsen et al., 2004; Etourneau et al., 2013; Vorrath et al., 2023), potentially in relation to the latitudinal and insolation and thermal gradients specifically associated with wind stress and upwelling (Denis et al., 2010). The integration of multiple records from the Atlantic sector of the Southern Ocean suggest there was some late Holocene cooling, driven by enhanced cold-water export from the Weddell Gyre as a cavity developed under the Ronne Filchner Ice Shelf, combined with a northward shift of the Southern Hemisphere westerly wind belt (Xiao et al., 2016). However, the changes within the Weddell Sea remain poorly understood and there is a lack of data to reconstruct past sea-ice evolution (Verleyen et al., 2011), particularly over the continental shelf.

To address this, we analysed a snow petrel (*Pagodroma nivea*) stomach-oil deposit, accumulated at a nesting site in the Heimefrontfjella region of Dronning Maud Land, northeastern Weddell Sea. Such deposits have been previously demonstrated to record palaeoenvironmental information (McClymont et al., 2022; Berg et al., 2019; Ainley et al., 2006) by tracking the biochemical signature of changes in snow petrel diet, which is in turn related to environmental characteristics of their feeding grounds including sea-ice extent and ocean productivity. Snow petrels have a close affinity with sea-ice during the breeding season (Delord et al., 2016; Ainley et al., 2006), as they feed in areas of intermediate sea-ice cover and switch between neritic (close to shore)

and pelagic (offshore) feeding grounds (Ainley et al., 1998; Ainley et al., 1984).

Modern end-member studies have shown that specific prey species (e.g. krill, fish and squid) can be separated based on their fatty acid composition and can be used to infer different sea-ice conditions in the foraging area. For example, Antarctic (*Euphausia superba*) krill are high in C_{14:0}, C_{16:0} and C_{18:1} fatty acids (e.g. Cripps et al., 1999), whereas squid are dominated by $C_{16:0}$ and fish by $C_{18:0}$ fatty acids (Lewis, 1966); reviewed in McClymont et al. (2022). However, some fish can also be high in $C_{18:1}$, especially $C_{18:1(n-9)}$ (e.g. the myctophid *Electrona carlsbergi*) (Connan et al., 2008). This broad framework allows us to distinguish between an Antarctic krill-rich diet, reflecting an offshore (pelagic) habitat, and a fish-rich diet, reflecting near-shore and continental shelf environments, based on the modern spatial distributions of fish (Ran et al., 2022; Liu et al., 2024; Freer et al., 2019), Antarctic krill (Mcbride et al., 2021) and cephalopod (mainly squid) (Xavier et al., 2016) species. Stable isotopes in stomach oils are also potentially excellent indicators of ecological baseline nutrient availability, trophic status (δ^{15} N) and the productivity and location of past foraging habitats (δ^{13} C) (Mc-Clymont et al., 2022; Ainley et al., 2006).

Using a radiocarbon-based age-depth model, we analyse a range of organic geochemical biomarkers (including the first analyses of phytol and cholesterol in stomach oil deposits), bulk elemental chemistry and stable isotopes in the stomach oil deposit from Heimefrontfjella. These record three distinctive periods of Holocene climate and sea-ice cover, which we compare with existing records of environmental changes in Antarctica and the Southern Ocean.

2 Materials and methods

2.1 Regional context

The Antarctic seasonal sea ice cycle is characterised by growth to maximum extent in September, followed by retreat to a minimum in February. Between the minimum and maximum sea-ice extents lies the Marginal Ice Zone (MIZ), characterised by sea-ice concentrations between 15 % and 80 %. In the northeastern Weddell Sea, the median sea-ice edge (15 % sea-ice concentration) retreats rapidly with spring melt. In October/November, when the snow petrels start to return to their nesting sites, the sea-ice edge is located north of 60° S. Rapid sea-ice retreat through December brings the sea-ice edge to $\sim 70^{\circ}$ S by early January, spanning the snow petrel incubation phase, then retreats further westward until the minimum in February (Fig. 1). The Weddell Sea gyre advects sea ice clockwise across the basin where it outflows in the northwest (Gupta et al., 2025). Sea ice tends to accumulate to the greatest extent in the south of the Weddell Sea due to this gyre (Hutchings et al., 2012).

The preferred foraging habitat of snow petrels has been observed to track the MIZ, where the presence of open waters

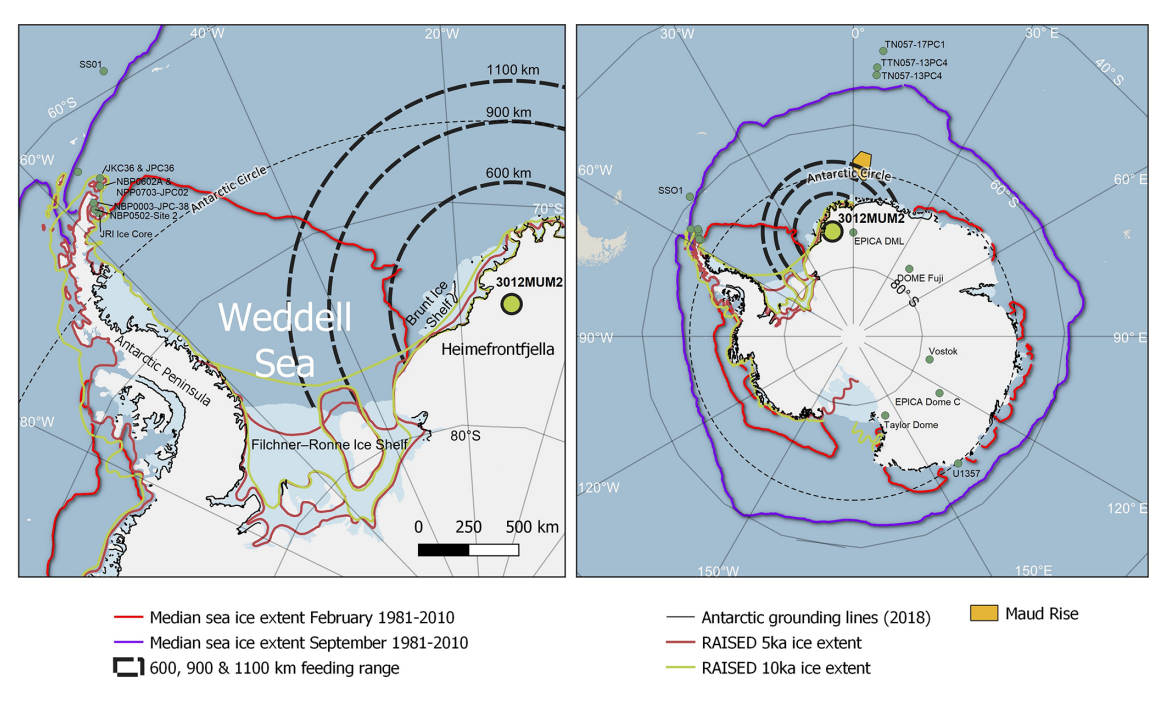


Figure 1. Location of Holocene snow petrel stomach oil record 3012MUM2, from Heimefrontfjella (74°34.14′ S, 11°15.02′ W; yellow circle) in the context of the Weddell Sea, and Antarctic Peninsula (left panel) and Antarctica and the Southern Ocean (right panel). Dashed black lines indicate sectors within 600, 900 and 1100 km snow petrel foraging range from the stomach oil deposit. Also shown are median modern sea ice extents in February and September (Fetterer et al., 2017), RAISED grounded ice sheet extents at 5 and 10 ka (Bentley et al., 2014) and inferred modern Antarctic grounding lines (Rignot et al., 2022). Other locations and core sites mentioned in the text include: ice cores from EPICA DML (Masson-Delmotte et al., 2011); Dome Fuji (Masson-Delmotte et al., 2011); EPICA Dome C (Masson-Delmotte et al., 2011); Vostok (Masson-Delmotte et al., 2011); Taylor Dome (Masson-Delmotte et al., 2011) and James Ross Island (JRI) (Mulvaney et al., 2012); marine sediment cores U1357 (Ashley et al., 2021); TTN057-13PC4 (Hodell et al., 2001); TN057-13PC4 (Divine et al., 2010; Nielsen et al., 2007); TN057-17PC1 (Divine et al., 2010; Nielsen et al., 2007); ANT28/D1–7 (Nie et al., 2022); NBP0003-JPC38 (Barbara et al., 2013); NBP0502-Site 2, Herbert Sound (Totten et al., 2015); NBP0602A and NPP0703-JPC02, Firth of Tay (Michalchuk et al., 2009; Majewski and Anderson, 2009); SS01 (Bak et al., 2007); and JKC36 and JPC36, Perseverance Drift (Kyrmanidou et al., 2018). Map developed using Quantarctica (https://www.npolar.no/quantarctica, last access: 15 October 2025).

within the sea ice facilitates access to prey (Wakefield et al., 2025). This foraging behaviour can see snow petrels foraging over and beyond the continental shelf, reaching ~ 700 – 1400 km from the nest site depending on the time of the breeding cycle and sea-ice extent (Honan et al., 2025). Based on regional tracking studies to the east, in Dronning Maud Land (Honan et al., 2025; Wakefield et al., 2025) three foraging options are available for snow petrels at Heimefrontfjella: (1) they head north to the MIZ lying to the south of the outer ice edge; (2) they head north east to the Maud Rise, where an intermittent open-ocean polynya and earlier sea ice melt provides foraging habitat; (3) they forage in the MIZ closer to the continental shelf, which can be associated with coastal polynyas. Tracking studies show that the most likely scenario is that early in the breeding season snow petrels forage in association with the northern edge of the MIZ as the sea ice retreats (Wakefield et al., 2025). As the sea-ice edge retreats so does the foraging range, so that later in the season snow petrels are more likely to be found in coastal waters (Honan et al., 2025; Wakefield et al., 2025).

2.2 Heimefrontfjella stomach oil deposit 3012MUM2

Stomach-oil deposit 3012MUM2 was collected in season 2014–2015 from the Boysennuten nunatak in the Heimefrontfjella Range (74°34.14′ S, 11°15.02′ W) (Fig. 1). The \sim 32 cm \times 23 cm deposit with a maximum thickness of 19 cm had an irregular, mamillated outer surface (Mc-Clymont et al., 2022). It was located immediately beneath a sheltered rock crevice, a typical habitat for nesting snow petrels, at an elevation of 1336 m above sea level (Fig. S1a and b in the Supplement). It was kept in the dark and frozen at -20 °C throughout the transportation processes to Durham University where sampling was carried out from 2021. The deposit was sliced using a circular saw while still frozen to preserve the internal millimetre-scale laminae which, when oriented, spanned a depth of \sim 19 cm along the cutting axis (Fig. S1c). Sub sampling was carried out at 2.5 mm resolution with 3.0 mm biopsy punches for organic geochemistry, isotopes and radiocarbon analyses. We selected a sampling line which represented the maximum accumulation rate and a continuous sequence through the stratigraphy; noting

Table 1. Radiocarbon dates including raw 14 C, F^{14} C and Bayesian calibrated ages for the 3012MUM2 sequence. Samples analysed by BETA Analytic (Florida) 14 C-AMS were prepared without acidification. Repeat analyses at 5 and 10.5 cm were prepared at SUERC Radiocarbon Laboratory using acidification and run for 14 C-AMS at UC Irvine Keck Carbon Cycle laboratory. A reservoir offset based on closest Holocene ΔR of 670 ± 50 years (Björck et al., 1991) was used, following previous studies (McClymont et al., 2022) and converted to calendar ages using the MARINE20 calibration (Heaton et al., 2020). All dates (14 C and calibrated) rounded to nearest 10 calendar years for presentation, original measured dates are available at Pangaea (https://doi.org/10.1594/PANGAEA.980519, Stevenson et al., 2025). The Bayesian model output is shown in Fig. 2.

Depth (cm)	AMS lab ID	Age (¹⁴ C yr BP)	$\pm (^{14}\text{C yr BP})$	F ¹⁴ C	Bayesian modelled calibrated age using P_sequence in OxCal (cal. yr BP)		
					Median	Max	Min
0.0	Beta – 679228	2510	30	0.7316	1260	1420	1060
1.0	Beta - 620905	3520	30	0.6452	2420	2670	2210
3.5	Beta - 679229	4630	30	0.5619	3780	4000	3560
5.0	Beta – 620906*	5030	30	0.5346	4240	4420	4050
5.0	UCIAMS-276896*	4958	35	0.5394	4240	4420	4050
5.5	Beta – 620907	4990	30	0.5373	4280	4450	4090
10.0	Beta - 620908	5520	30	0.5030	4940	5150	4770
10.5	Beta – 620909*	5610	30	0.4974	4990	5200	4820
10.5	UCIAMS-276897*	5490	35	0.5048	4990	5200	4820
13.5	Beta - 620910	5910	30	0.4792	5430	5600	5250
17.0	Beta - 620911	6720	30	0.4332	6280	6440	6100
18.5	Beta – 679230	6840	30	0.4268	6410	6610	6250

^{*} Bayesian P-Sequence model applies single age to paired date due to R_Combine function in OxCal.

some heterogeneity either side of this line (Figs. 2c and S1c). A 19 cm long slice from the opposite face of the cut was mounted in plastic trunking for high-resolution X-ray fluorescence (XRF) analysis of elemental composition.

2.3 Radiocarbon analyses and age-depth modelling

An age-depth model for 3012MUM2 was constructed from twelve ¹⁴C ages (Table 1). The top and bottom ages were sampled at 0 and 18.5 cm, immediately above and below the first geochemical samples (0.5 and 18.25 cm, respectively). Most of the radiocarbon ages were carried out by Beta Analytic (Miami, USA) using ¹⁴C-AMS via graphitization on untreated samples, which were oxidised to CO₂ by combustion in O₂ and converted to graphite with Co powder as a catalyst. To assess for the effects of acid removal on ¹⁴C ages samples at 5.0 and 10.5 cm were repeat-sampled and analysed at SUERC (Scottish Universities Environmental Research Centre) Environmental Radiocarbon Laboratory by digestion in 1 M HCL (hydrochloric acid) (at 80 °C, 2 h), washed free of mineral acid with deionised water, dried and homogenised. Carbon was recovered from the residue as CO₂ by heating with CuO in a sealed tube and converted to graphite by Fe/Zn reduction. Samples were then analysed by AMS at the Keck Carbon Cycle AMS Facility, University of California, Irvine, USA. For calibration of radiocarbon ages to calendar ages (Table 1) the MARINE20 radiocarbon age calibration (Heaton et al., 2020) was used, taking into account the regional marine reservoir of $\Delta R = 670 \pm 50$ years, measured at Hope Bay in the western Weddell Sea (Björck et al., 1991). This approach has previously been applied to snow petrel stomach-oil deposits (McClymont et al., 2022). A Bayesian age-depth model was then built in OxCal v4.4 (Bronk Ramsey, 2009) using the default settings (applied with a general outlier model, except for paired dates where we used the *SSimple* outlier model). Our choice of a Bayesian approach to age-depth modelling means that the age uncertainties of all dates are considered for the entire age model.

2.4 Bulk stable isotope analysis and organic matter elemental composition

Carbon and nitrogen stable isotope analysis was performed using a Costech ECS400 elemental analyser coupled to a Thermo Scientific Delta V Advantage isotope ratio mass spectrometer in the Stable Isotope Biogeochemistry Laboratory (SIBL) at Durham University. The method used is described in McClymont et al. (2022). Results are reported in standard delta (δ) notation in per mil (δ) relative to Vienna Pee Dee Belemnite (VPDB) and atmospheric nitrogen (AIR), respectively. The linear range for δ ¹³C was between -46% and +3% and for δ ¹⁵N between -4.5% and +20.4%, based on daily analysis of international (e.g. IAEA-600, IAEA-CH-3, IAEA-CH-6, IAEA-N-1, IAEA-N-2, NBS 19, USGS24, USGS40) and in-house standards, enabling a 2-standard-deviation analytical uncertainty of \pm 0.1% for in-

ternational standards (replicated) and $<\!\pm\,0.2\,\%$ on replicated samples. Total carbon (wt % C) and nitrogen (wt % N) were obtained simultaneously using an internal standard of glutamic acid (40.8 wt % C; 9.5 wt % N).

2.5 Biomarker analyses

The biomarker sub-samples (0.02-0.05 g) were extracted in 4 mL dichloromethane (DCM): hexane (3:1) after addition of internal standards (nonadecane, heptadecanoic acid, 5α androstane, 5α -androstanol) and then sonicated for 15 min. Extracts were decanted and the procedure was repeated three more times. Extracts were combined and taken to dryness using rotary evaporation and N2. The entire sample was then saponified using 1 mL KOH (8 %) in methanol (95 %), heated for 1 h at 70 °C and left overnight. The neutral fraction was extracted with 3×3 mL hexane. The remaining sample was acidified to pH < 3 using drops of 2 M HCL, followed by extraction of fatty acids with hexane and evaporation to dryness with N₂. Fatty acid methyl esters (FAMEs) were generated by methylating the fatty acid fraction using 3 mL methanol: HCL (95:5) heated for 12 h and left to cool. Samples were rinsed with 4 M DCM-cleaned H₂O and then FAMEs were extracted with at least three DCM: hexane rinses (4:1), before evaporation to dryness under N2. Neutral fractions were separated in up to four fractions using 4 cm deactivated silica (heated 140 °C for 16 h) columns in glass pipettes plugged with extracted cotton wool (silica pore size 60 Å, 220–240 mesh particle size; 35–75 µm particle size; Sigma-Aldrich 60738-1KG). Hexane was used to condition the columns (x3 column volumes) followed by injection of the sample dissolved in 500 µL DCM directly into the column. Elution order into separate fractions used three column volumes each of hexane, DCM, DCM: methanol (1:1) and methanol. All fractions were decanted and transferred into GC vials and evaporated to dryness using N2. Fraction F3 (DCM: methanol (1:1), which recovered nalcohols, phytol and sterols, was then further derivatized to trimethylsilyl esters prior to analysis using 50 µL DCM and 50 μL BSTFA (N,O-Bis(trimethylsilyl)trifluoroacetamide) (with 1% TMCS (chlorotrimethylsilane)) heated for 1h at 70 °C and left overnight prior to analysis. Samples were evaporated to dryness and dissolved in hexane prior to analysis.

All extracts were analysed using a Thermo Trace 1310 gas chromatograph coupled to an ISQ LT single quadrupole mass spectrometer (GC-MS). FAMEs extracts were separated using a Restek FAMEWAX (crossbond polyethylene glycol) column (30 m \times 0.25 mm \times 0.25 µm), similar to McClymont et al. (2022) but with some modifications. Briefly, samples were injected (0.8 µL) into a programmable temperature vapouring (PTV) injector in CT Splitless mode with inlet temperature at 250 °C, carrier gas in constant flow and with helium carrier gas set to 1.5 mLmin $^{-1}$ (split flow 15.0 mLmin $^{-1}$; splitless time 1.5 min; purge flow

5.0 mL min⁻¹). GC oven temperature was set to 100 °C for 3 min followed by 2 °C min⁻¹ to 230 °C; hold of 12 min. Prep-run timeout was 10 min and equilibration time 0.5 min. MS settings included: transfer line, 230 °C; ion source temperature, 230 °C, mass range 38 to 600 *m/z* (every 0.5 s). Compounds were identified from their respective mass spectra and retention times, with quantities calculated relative to the peak area of the internal standard heptadecanoic acid and an assumption of a 1 : 1 response (validated by comparison with Supelco 37 component FAME mix; CRM47885, Merck).

Fraction F3 (previously eluted in DCM: methanol (1:1)) was separated using a Restek Rxi-5ms (crossbond 5% diphenyl/95% dimethyl polysiloxane) column $(60 \,\mathrm{m} \times 0.25 \,\mathrm{mm} \times 0.25 \,\mathrm{\mu m})$. Similarly, samples were injected (0.8 µL) into a programmable temperature vapouring (PTV) injector in CT split-less mode but at 280 °C inlet temperature, with helium carrier gas set to 2.3 mL min⁻¹ set in constant flow mode (split flow set to 23 mL min⁻¹; splitless time 1 min; septum purge flow 5.0 mL min⁻¹). GC oven temperature was set to 50 °C hold for 2 min followed by 10 °C min⁻¹ to 200 °C; followed by a slower ramp of 3 °C min⁻¹ to 300 °C and a hold of 20 min (prep run timeout was 10 min, equilibration time 0.5 min). MS settings included: transfer line, 310 °C; ion volume, 300 °C, mass range 50 to $550 \, m/z$ (every 0.5 s). Compounds were identified from their respective mass spectra and retention times, with quantities of trimethylsilyl esters (TMS) calculated relative to the peak area of the internal standard 5α -androstanol and an assumption of a 1:1 response (validated by identically derivatized standard mix which included cholesterol-TMS).

2.6 XRF analyses

XRF (X-ray fluorescence) analysis was carried out at Durham University, Department of Geography using a GEOTEK XRF Core Workstation (MSCL-XYZ) equipped with a rhodium source X-ray generator with a 10 mm crosscore slit width and a 1 mm downcore window. During operation the XRF scanner was set to analyse four different beam conditions, with a counting time of 10 s per beam. Beam conditions applied to the generator included: (1) no filter, 10 kV; (2) 25 μm silver filter, 20 kV; (3) 125 μm silver filter, 30 kV; (4) 625 μm copper filter, 50 kV. Detector measurement of photons ranged 2–35 keV. To pre-screen complex data, including removal of missing values and selecting elemental compositions from the most appropriate beam, the R 3.6.0 package "tidyverse" (Wickham et al., 2019) was used to produce a master XRF dataset.

2.7 ICP-OES analysis

To determine local bedrock chemistry, a sample of gneissic granite rock (consistent with local geology; Juckes, 1972) attached to deposit 3012MUM2 was soaked in ethanol to re-

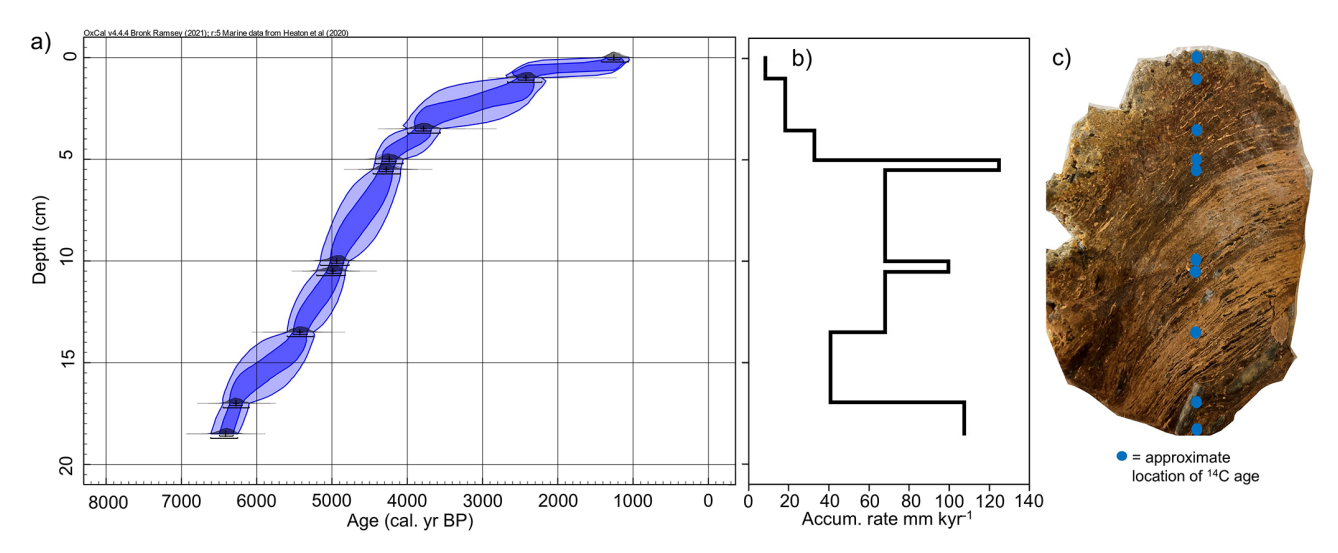


Figure 2. (a) Bayesian 14 C-AMS age-depth model for stomach oil deposit 3012MUM2, generated in OxCal (Bronk Ramsey, 2009) applying a reservoir offset ($\Delta R^{\text{Holocene}}$ 670 \pm 50 years (Björck et al., 1991) calibrated to calendar ages using MARINE20 (Heaton et al., 2020). Dark blue ellipse indicates 68.3 % range, light blue ellipse indicates 95.4 % range. (b) Accumulation rate between age control points calculated from median ages in the Bayesian model in (a). (c) Photograph of stomach oil deposit 3012MUM2 after sectioning, complete with approximate location of 14 C ages in blue dots. Constrained hierarchical cluster analysis was used to determine three significant clusters (Org A–C) using organic parameters in rioja (Juggins, 2020) and the broken-stick model (Bennett, 1996).

move stomach-oil residue (repeated 3–4 times). It was then crushed using a fly press, freeze dried for 48 h, and ground to a fine, homogenous powder using a ball mill. Organic matter was removed by adding 4 mL of 30 % hydrogen peroxide to a $\sim 0.5\,\mathrm{g}$ aliquot of rock. The sample was then digested for 4 h in 16 mL of Aqua Regia using a DigiPREP digestion block, and subsequently diluted to 50 mL with deionised water and filtered at 0.45 μm . Elemental composition was determined using an Agilent Technologies 5100 Inductively Coupled Plasma Optical Emissions Spectrometer (ICP-OES).

2.8 Statistical and numerical analyses

Cluster analysis was carried out to highlight changes in geochemistry between neighbouring units in both inorganic (XRF) and organic (stable isotopes, TOC, C/N ratio and biomarkers) parameters with depth. For each dataset (organic (Org A–C) and inorganic (XRF A–C), separately) a constrained hierarchical cluster analysis based on sample order was performed using the *rioja* package in R (Juggins, 2020). A broken stick analysis (Bennett, 1996) was used to identify the maximum number of statistically significant clusters.

Principal components analysis (PCA) was carried out in Canoco V.5.51 (Ter Braak and Smilauer, 2002) on \log_{10} -transformed and centred data: the inorganic (XRF) and organic (bulk organic geochemistry and biomarkers) parameters were treated separately. Input data for the organic PCA included bulk organics and biomarker concentrations, rather than fluxes (which included TOC normalized data and ratios). Input data for the inorganic PCA included XRF units in counts per second, rather than fluxes. As most XRF pa-

rameters had samples with counts < 500 we chose to retain all parameters that had passed the pre-screening process (see Sect. 2.5 XRF analyses). The lists of elements and compounds used in inorganic and organic PCA are shown in Tables S1 and S2 in the Supplement.

3 Results

3.1 Stomach-oil deposit 3012MUM2 age model

The stomach-oil deposit 3012MUM2 spans 1260 (1060–1420) cal. yr BP at 0 cm to 6410 (6250–6610) cal. yr BP at 18.5 cm (Table 1, Fig. 2a). When taking biomarker and isotope samples we avoided the margins of the deposit, which were easily deformable. As a result, the oldest and youngest biomarker and isotope samples lie at 0.5 cm (1830 (1170–2530) cal. yr BP) and 18.25 cm (6390 (6210–6590) cal. yr BP), respectively in the Bayesian model, or ~1800 to 6400 cal. yr BP when rounded to closest 100 years. The accumulation rate based on the median Bayesian modelled age between radiocarbon dating depths varied between 8.6 and 125.0 mm kyr⁻¹ (Fig. 2b).

3.2 Compositional changes in bulk organic matter and stable isotopes

The 3012MUM2 samples were high in organic C (36.6 %–68.3 %; mean 49.8 %) and total N (2.9 %–16.8 % (mean 9.7 %) (Fig. 3). The C: N_{atomic} ratio varied between 3.4 and 20.8 (mean 7.5). Bulk δ^{13} C had a narrow range from -31.0% to -29.5%, with a mean of -30.3% and a very

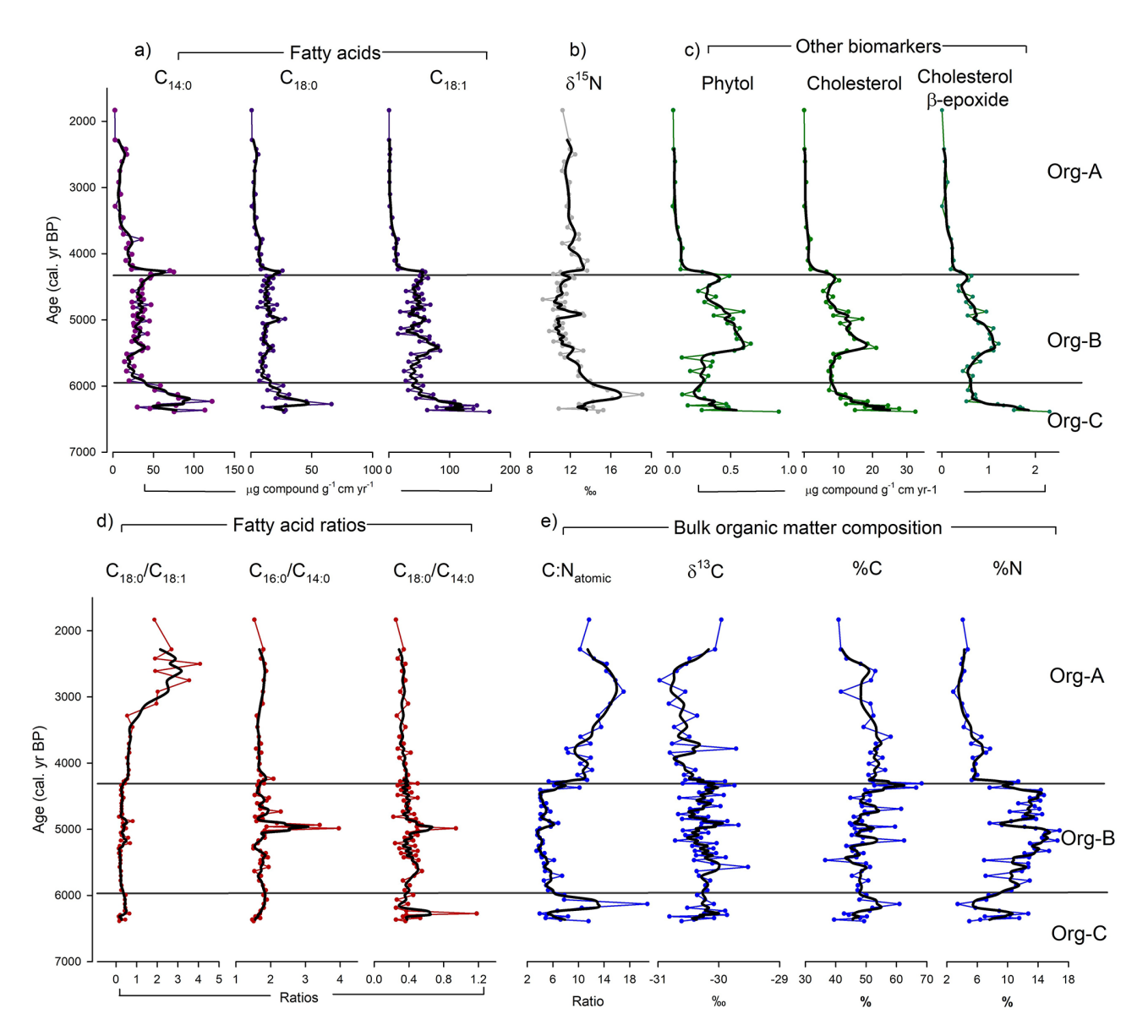


Figure 3. Organic parameters as fluxes and ratios measured in stomach oil deposit 3012MUM2, plotted against the age-depth model (Fig. 2). Smooth lines in bold are 3-point moving averages. Constrained hierarchical cluster analysis was used to determine three significant clusters (Org A-C) using organic parameters in rioja (Juggins, 2020), compared with the broken-stick model (Bennett, 1996). (a) Fatty acid concentrations ($C_{14:0}$, $C_{18:0}$, $C_{18:1(n-9)}$); (b) nitrogen stable isotopes (δ^{15} N); (c) Other biomarkers (phytol and cholesterol); (d) Fatty acid ratios ($C_{18:0}/C_{18:1(n-9)}$, $C_{16:0}/C_{14:0}$, $C_{18:0}/C_{14:0}$); e) other measures of bulk organic matter composition ($C:N_{atomic}$ ratio, δ^{13} C, % C and % N).

small standard deviation (SD) of 0.3% (Fig. 3). In contrast bulk δ^{15} N had a wide range between 9.3% and 19.1% (mean 12.2%, SD 1.6%) (Fig. 3).

3.3 Compositional changes in biomarkers

Here and in the discussion, we present the majority of biomarkers as fluxes (Fig. 3). Given similar patterns with biomarker concentrations (Figs. S2–S4) we consider the trends we have identified to be robust. The 3012MUM2 deposit samples likely comprised wax esters consistent with ex-

isting stomach oil studies (Imber, 1976; Lewis, 1966, 1969; Warham et al., 1976; Watts and Warham, 1976), and contributions from free lipids. Once saponified and derivatised, the extracts were dominated by fatty acids (FA) and alcohols (FAlc) (Fig. S3). In 3012MUM2, $C_{16:0}$ was the most abundant fatty acid (mean $38.9\% \pm 8.8\%$ SD), followed by $C_{18:1(n-9)}$ (FA) (mean $23.6\% \pm 10.9\%$ SD), $C_{14:0}$ (FA) (mean $22.1\% \pm 5.2\%$ SD), $C_{18:0}$ (FA) (mean $8.4\% \pm 2.1\%$ SD) and $C_{16:1}$ (FA) (mean $7.1\% \pm 3.5\%$ SD).

By flux, FA were most abundant ($C_{14:0}$, $C_{16:0}$, $C_{16:1}$, $C_{18:0}$, $C_{18:1(n-9)}$) (total mean $182.25 \,\mu g \,g^{-1} \,cm \,yr^{-1}$,

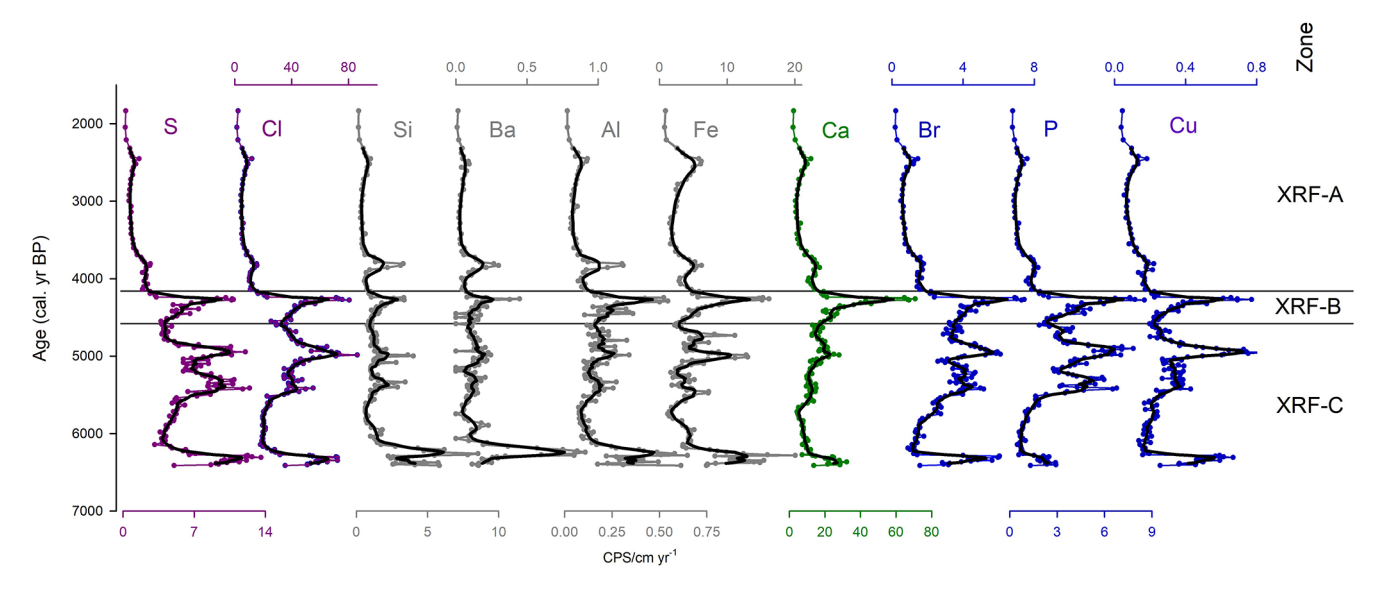


Figure 4. Key inorganic elements measured in stomach-oil deposit 3012MUM2, plotted as qualitative counts per second (cps) normalised to accumulation rate, to approximate element fluxes against the age-depth model (Fig. 2). Elements include S, Cl, Si, Ba, Al, Fe, Ca, Br P and Cu. Plots are coloured according to groupings on the PCA. Black lines indicate 7-point moving averages. Cluster boundaries (XRF-A, B and C) and XRF PCA are uniquely calculated from entire XRF dataset (Fig. S3).

SD $116.69 \,\mu g \,g^{-1} \,cm \,yr^{-1}$) followed by *n*-alkanols $(C_{14:0},\ C_{16:0},\ C_{18:0},\ C_{20:0}$ and $C_{22:0})$ (FAlc) (total mean $47.95 \,\mu g \, g^{-1} \, cm \, yr^{-1}$, SD $44.33 \,\mu g \, g^{-1} \, cm \, yr^{-1}$). The other compounds were less abundant, with cholesterol the highest (mean $9.95 \,\mu g \,g^{-1} \,cm \,yr^{-1}$, SD $7.47 \,\mu g \,g^{-1} \,cm \,yr^{-1}$) and phytol in lower concentrations (mean $0.31 \,\mu\mathrm{g}\,\mathrm{g}^{-1}\,\mathrm{cm}\,\mathrm{yr}^{-1}$; $0.22 \,\mu g \, g^{-1} \, cm \, yr^{-1}$). Phytol is formed from the ester-linked side chain of chlorophyll a and can therefore primarily be considered a biomarker for phytoplankton (Rontani and Volkman, 2003). Cholesterol is a ubiquitous marker but in this context could be considered a krill marker (both Antarctic and ice krill), since it can account for more than 76% of total sterols in krill (Ju and Harvey, 2004) and is typically lower in concentration in fish (e.g. cholesterol in Dissostichus mawsoni ranges 4.7 %–14.3 % of total lipids; Clarke, 1984). We also assessed the distributions of sterols (e.g. 22-dehydrocholesterol), stanols (e.g. coprostanol) and cholesterol derivatives (e.g. cholesterol α/β -epoxide); cholesterol was the most abundant contributor (Fig. S4).

During saponification of the relevant wax esters, n-alkanols (FAlc) were also formed with saturated even chain lengths; $C_{14:0}$ (FAlc) to $C_{22:0}$ (FAlc) n-alcohols were the most abundant (Fig. S3). Amongst the n-alcohols $C_{16:0}$ (FAlc) was the most abundant (mean $63\% \pm 2.9\%$ SD), followed by $C_{14:0}$ (FAlc) (mean $22.4\% \pm 1.8\%$ SD) and $C_{18:0}$ (FAlc) (mean $13.0\% \pm 2.1\%$ SD). $C_{20:0}$ (FAlc) (mean $1.3\% \pm 0.4\%$ SD) and $C_{22:0}$ (FAlc) (mean $0.3\% \pm 0.1\%$ SD) n-alcohols were relatively minor contributors.

Broadly, PC axis 1 (30% variance explained) for the organic geochemistry indicators had high positive loadings in C: N ratio and $C_{18:0}/C_{18:1(n-9)}$ (FA), while PC axis 2 (24%)

variance explained) had strong positive loadings in $C_{16:0}$ (FA), $C_{18:0}$ (FA), $\delta^{15}N$ and C:N ratio (Table S2 and Fig. S9).

3.4 Changes in biomarkers through time

Cluster analysis identified three statistically significant organic zones (Org-A, B and C) which are used as a framework to discuss the changes in key biomarkers through time. Although clusters were identified from organic analyses, there were 8 zones of colour visible in 3012MUM2 (Fig. S1c). In terms of lithological units, zone Org-C closely matched with zone 8 (darkest layer, black/brown), with zones 4–7 matching most closely with zone Org-B (lighter, yellowy/orange) and zones 1–3 matching with Org-A (medium-dark, grey brown to black brown).

3.4.1 Organic Zone – C (\sim 6390–5960 cal. yr BP)

The base of the deposit is marked by relatively high fatty acid (FA) fluxes: $C_{14:0}$ (FA), $C_{18:0}$ (FA) and $C_{18:1(n-9)}$ (FA) increased to maxima around $\sim 6300\,\mathrm{cal.yr\,BP}$ and declined by the top of the zone (5960 cal.yr BP) (Fig. 3). This is broadly coincident with a pulse of high $\delta^{15}N$ (reaching $\sim 20\,\%$ o, $\sim 6100\,\mathrm{cal.yr\,BP}$), which follows the trend in $C_{14:0}$ (FA) but is slightly offset (Fig. 3). Ratios of fatty acids $C_{18:0}/C_{18:1(n-9)}$ and $C_{16:0}/C_{14:0}$ remained low, with a pulse in $C_{18:0}/C_{14:0}$ (FA) reaching a maximum at $\sim 6300\,\mathrm{cal.yr\,BP}$ (Fig. 3). A peak of $60\,\%$ C $\sim 6100\,\mathrm{cal.yr\,BP}$ is reflected in the maximum C: N_{atomic} ratio value of ~ 21 (Fig. 3). δ^{13} C fluctuated between $-29.9\,\%$ o and $-30.8\,\%$ o. Phytol and cholesterol were relatively high with phytol fluctuating between

0.06 and 0.6 μ g g⁻¹ cm yr⁻¹ and cholesterol between 0.3 and 1.6 μ g g⁻¹ cm yr⁻¹ (Fig. 3). All *n*-alkanols (FAlc) increased to higher concentrations around \sim 6200 cal. yr BP (Fig. S3). Most other biomarkers of sterols, stanols and cholesterol derivatives were generally high in this zone (Fig. S3).

3.4.2 Organic Zone − B (~5960–4320 cal. yr BP)

The transition to zone B (\sim 5960 cal.yrBP) is marked by a rapid decrease in $C_{14:0}$ (FA), $C_{16:0}$ (FA) and $C_{18:0}$ (FA) fatty acid fluxes which thereafter remained broadly stable throughout the zone (Figs. 3, S2). Zone Org-B has markedly lower δ^{15} N than zone Org-C, fluctuating between $\sim 9\%$ and 13%. In contrast, the $C_{16:1}$ (FA) and $C_{18:1(n-9)}$ (FA) fatty acid concentrations decreased from around 5400 cal. yrBP to the top of zone Org-B, which is also observed in phytol and cholesterol from \sim 5100 cal. yr BP (Figs. S2 and S3). The major n-alkanols were markedly lower in zone Org-B compared to zone Org-C (Fig. S3), with a similar trend to lower values in C: N_{atomic} ratio (Fig. 3). Notably, at ~ 4900 cal. yr. BP there was a short-lived unusual interval of high δ^{15} N, high $C_{16:0}/C_{14:0}$ (FA), $C_{18:0}/C_{14:0}$ (FA) and a small increase in C: N ratio (Fig. 3). Organic carbon composition was variable in zone Org-B, fluctuation between -30.7%to -29.5% for δ^{13} C, and between $\sim 36.6\%$ to 66% for %C (Fig. 3). Other biomarkers of sterols, stanols and cholesterol derivatives were generally high at the bottom of zone Org-B (\sim 5960 cal. yr BP), typically decreasing by the top $(\sim 4320 \text{ cal. yr BP})$ (Fig. S4).

3.4.3 Organic Zone − A (~4320–1830 cal. yr BP)

For most biomarkers zone Org-A is a relatively stable period, with fluxes and concentrations of C_{14:0} (FA), C_{18:0} (FA) and C_{18:1(n-9)} (FA) remaining low, broadly similar to the previous zone Org-B. The fatty acid ratios C_{16:0}/C_{14:0} and $C_{18:0}/C_{14:0}$ are stable throughout (Figs. 3, S2 and S3). Between 4000 and 4320 cal. yr BP, δ^{15} N was slightly higher (reaching 13.7%) before decreasing towards the top of the deposit (Fig. 3). $C_{14:0}$ (FAlc), $C_{16:0}$ (FAlc) and $C_{18:0}$ (FAlc) *n*-alkanols also reached maxima at ~ 3800 cal. yr BP (Fig. S3). $C_{16:1}$ (FA) and $C_{18:1(n-9)}$ (FA) concentrations were markedly lower than zone Org-B, and decreased further to the top of zone Org-A (Figs. S2 and S3), with a similar trend in C_{18:1(n-9)} (FA) fluxes (Fig. 3). Of note, after \sim 3300 cal. yr BP $C_{18:0}/C_{18:1(n-9)}$ (FA) ratios increased, and reached a maximum of ~ 4 at 2500 cal. yr BP. Similarly, C: N_{atomic} gradually increased to a maximum of ~ 17 by ~ 2900 cal. yr BP, before decreasing to the top of the sequence (~ 11.7), while δ^{13} C displayed the reverse trend (increasing from $\sim -31\%$ at ~ 2700 cal. yr BP to -29.9%at the top of the sequence) (Fig. 3). Phytol and cholesterol were relatively low in zone Org-A, and both displayed trends of decreasing concentrations to the top of the sequence (Fig. 3). Other biomarkers of sterols, stanols and cholesterol derivatives were similarly also low throughout zone Org-A (Fig. S4).

3.5 Inorganic composition (XRF)

Cluster analysis identified three major XRF clusters: XRF-C (6390–4570 cal. yr BP); XRF-B (4570–4180 cal. yr BP); XRF-A (4180–1830 cal. yr BP). Zone XRF-C broadly coincides with organic zone Org-C and B, with XRF-B aligning (although slightly offset) with the uppermost part of zone Org-B. Zones XRF-A and zone Org-A are broadly aligned.

Based on XRF mean counts per second (cps) the largest elemental contributors to stomach-oil deposit 3012MUM2 were Cl, Ca, Fe, S, K, Br and P. Key XRF-derived inorganic compositions normalised to accumulation rate are presented in Fig. 4. Fluxes are characterised by higher variability in XRF-C with peaks in multiple elements at $\sim\!6300,\sim5300-4900\,\mathrm{cal}$. yr BP and at the top of the zone ($\sim\!4570\,\mathrm{cal}$. yr BP). In XRF-B values reach a peak at $\sim\!4300\,\mathrm{cal}$. yr BP. Elemental fluxes are lower and relatively stable in XRF-A, with a small peak in some elements such as Fe $\sim\!2400\,\mathrm{cal}$. yr BP.

Based on the PCA of counts per second data, PC1 reflected 28 % of the variance (Table S1; Fig. S10) and included Si, Ba Al and Fe, which tend to peak around $\sim 6300\,\text{cal.yr\,BP}$ in zone XRF-C (Fig. S5). PC2 reflected 22 % of variance (Table S1; Fig. S10), and included S, Cl, Br, P and Cu, which shift towards lower values and lower variability in XRF-A (Fig. 4).

4 Discussion

We found pronounced variations in geochemical proxies in stomach-oil deposit 3012MUM2 showing snow petrel diet was responding to changes in sea-ice conditions and ocean productivity related to changes in ice sheet extent and climate. In this discussion we first outline the rationale and caveats in our proxy interpretations, then explain the links between diet changes and sea ice environments through time.

4.1 Proxy interpretations

High levels of organic C and N in 3012MUM2 were similar to previously measured snow petrel stomach oil deposits (e.g. McClymont et al., 2022; Berg et al., 2023; Hiller et al., 1988), while bulk δ^{13} C values were within the range of previous measurements of a Holocene deposit (Ainley et al., 2006). The fatty acid (FA) distributions found in the stomach oils are commensurate with previous stomach-oil and source endmember studies which suggest a diet of krill (mainly $C_{14:0}$ (FA), $C_{16:0}$ (FA)), squid ($C_{16:0}$ (FA)) and fish ($C_{16:0}$ (FA), $C_{18:1(n-9)}$ (FA)) (Cripps et al., 1999; Lewis, 1966) as summarised in McClymont et al. (2022) and further explored in Berg et al. (2023). While some FAs are labile and susceptible to degradation, particularly unsaturated FAs (Stefanova and Disnar, 2000), the similar profiles shown by $C_{14:0}$ and

 $C_{18:0}$ FA with $C_{18:1(n-9)}$ FA suggests that changes in diet, not preservation, is the main driver for the latter FA (Fig. S3).

In the PCA biplots for the XRF analysis (Table S1 and Fig. S10) negative loadings from elements which are commonly associated with seabirds (e.g. P, Zn, Sr, Ni), including Cu (Shatova et al., 2016; Shatova et al., 2017; Castro et al., 2021; Sparaventi et al., 2021) support our interpretation of dietary sources to the deposit (Duda et al., 2021). In contrast, the positive loading of Fe, Al, Si and Ca on PC1 aligns with the main elements measured in the rock specimen taken from 3012MUM2 (Table S3), which reflects the local gneissic granite bedrock (Juckes, 1972). These elements are interpreted to reflect locally-derived, probably bedrock, erosional contribution. Cu was also present in 3012MUM2, which is known to be a key Antarctic krill marker as a Cu backbone structure is found in hemocyanin (Bridges, 1983) and has been observed in previous snow petrel deposits to be associated with Antarctic krill (McClymont et al., 2022). Broadly elevated Cu in zone Org-B with elevated $C_{14\cdot0}$ FA and cholesterol (Fig. 3) also supports an Antarctic krill source for these components.

A wide range of $\delta^{15}N$ values is recorded, which could reflect environmental change (e.g. changing circulation, degradation) or dietary change (e.g. baseline values in phytoplankton, trophic level). Past variations in the $\delta^{15}N$ of circumpolar deep water (CDW) which upwells to the sea surface can contribute to high $\delta^{15}N$ (Kemeny et al., 2018), but it is so far unknown if this occurred during the timescale of our deposit between 6390 and 1830 cal. yr BP (as opposed to glacialinterglacial timescales). Fragmented coral $\delta^{15}N$ records of upper CDW indicate mid- to late Holocene values spanning $\sim 7\%c-11\%c$ (Chen et al., 2023) but without the resolution to compare shorter-term changes with the variations we observed in 3012MUM2. Diatom-bound records of baseline δ^{15} N show a long-term decline through the Holocene as nutrient availability has increased (e.g. Ai et al., 2020; Studer et al., 2018), which aligns in part with our overall trend. Previous work has cautioned that guano could contribute to stomach-oil deposits (Berg et al., 2019), which would also elevate $\delta^{15}N$ (e.g. Wainright et al., 1998; Bokhorst et al., 2007). Finally, weathering would also elevate δ^{15} N values due to microbial biosynthetic pathways causing ¹⁴N release (Macko and Estep, 1984). However, we only identified minor contributions from microbial fatty acids in 3012MUM2 to support this interpretation. In our discussion below, we focus on the environmental and dietary information provided by δ^{15} N in combination with other proxy indicators.

We focus mainly on organic compounds for interpretation of palaeoclimate because dietary lipids and organic isotopes reflect the main snow petrel dietary sources which can, in turn, provide secondary information on sea ice distribution (e.g. McClymont et al., 2022). In particular, we focus on $C_{14:0}$ (FA) as an indicator of past Antarctic krill contributions to the diet, $C_{18:0}$ (FA) for fish, $C_{18:1(n-9)}$ (FA) for mainly fish, bulk $\delta^{15}N$ as primarily an indicator of trophic status and

productivity, and phytol as an indicator of past productivity. In terms of past ice configurations, we interpret a diet with more Antarctic krill and high productivity as recording snow petrels feeding in the open ocean (within the MIZ or the open ocean) (e.g. zone Org-C). Zones of higher productivity with reduced Antarctic krill contributions are inferred to represent enhanced snow petrel feeding closer to shore, in neritic zones, either due to a more proximal MIZ or in coastal polynyas along the Antarctic ice sheet margin (e.g. zone Org-B). While zones with lower productivity and accumulation rates reflect sea ice expansion, a less accessible MIZ and a more dense ice pack (e.g. zone Org-A).

4.2 Interpreting changes in sea ice in mid-Holocene stomach-oil deposits

By the start of the 3012MUM2 record at \sim 6400 cal. yr BP, the Filchner and Ronne Ice Shelf had reached its modern position (Nichols et al., 2019; Johnson et al., 2019; Hillenbrand et al., 2017; Grieman et al., 2024). In other parts of Antarctica, cooling of the surface ocean and freshening of shelf surface waters since the middle-Holocene (Ashley et al., 2021) led to increased sea-ice concentrations and sea-ice duration over the continental shelf (Crosta et al., 2008; Mezgec et al., 2017; Johnson et al., 2021). Further offshore, sea ice became less extensive since ~ 6500 cal. yr BP (Nielsen et al., 2004; Xiao et al., 2016), reflecting shifts in the latitudinal insolation and thermal gradients (Denis et al., 2010) as well as the multi-centennial expression of climate modes, such as ENSO (El Niño-Southern Oscillation) (Crosta et al., 2021). For the wider Southern Ocean, exemplified in East Antarctica, after 4500 cal. yr BP although sea ice and turbulence persisted in locations proximal to the ice shelf, it did not increase further offshore due to northward transport of subpolar surface waters as a response to southern Westerlies reinforcement (Denis et al., 2010).

The evolution of Holocene sea ice has been separated into three distinct phases around Antarctica (Early Holocene ~ 11.5 to ~ 8 ka BP; mid-Holocene ~ 7 to $\sim 4-3$ ka BP; the late Holocene $\sim 5-3$ to 1-0 ka BP), with the phasing of these periods differing depending on regional response to long-term forcing (Crosta et al., 2022). Despite this wider knowledge there is an absence of any paleoenvironmental reconstructions of sea ice for the Holocene within the Weddell Sea region. Here we explore how each of the three statistically significant geochemical zones in the stomach oil deposit align with the timing or direction of the environmental shifts recorded by Crosta et al. (2022) and similar studies elsewhere in Antarctica.

4.2.1 Zone Org-C (6390–5960 cal. yr BP)

Between 6390–5960 cal. yr BP we infer that the snow petrels at Heimefrontfjella had a mixed diet which reflected access to areas of high productivity similar to today, with a MIZ

situated in pelagic waters but with the potential for foraging over the continental shelf when the MIZ was situated closer to the coast. This interpretation is based on geochemical evidence of a diet sporadically high in either Antarctic krill (Euphausia superba) (evidenced by FA $C_{14:0}$, Cu: pelagic waters) or fish (evidenced by $C_{18:0}$ (FA): continental shelf waters). While we are unable to constrain sea-ice extent precisely, we interpret the high but variable snow petrel stomach oil accumulation rates to reflect repeated nest occupation from an accessible foraging habitat. The MIZ must therefore have been located within the modern snow petrel foraging range i.e. within $\sim 1200\,\mathrm{km}$ from Heimefrontfjella (Fig. 1; Wakefield et al., 2025).

We acknowledge that there are intervals in zone Org-C when the C_{14:0} FA record does not align with Cu and cholesterol, which are instead positively correlated with indicators of guano: S and N (Cheng et al., 2016; Tatur et al., 1997; Roberts et al., 2017; Sun et al., 2000; Liu et al., 2005). The negative relationship between C: N and other elements (Cl, P, S) (Figs. S7 and S8) also supports a contribution from guano (Berg et al., 2019; Hiller et al., 1988). Although the presence of guano is unlikely to be an issue for interpreting dietary changes, as different biomarkers are involved (e.g. FA $C_{14:0}$, FA $C_{16:0}$, FA $C_{18:1(n-9)}$ for diet), it may have contributed to the elevated bulk $\delta^{15}N$ values in zone Org-C. The δ^{15} N values are exceptionally high in zone Org-C ($\sim 20\%$), exceeding those observed in modern Southern Ocean top predators ($\sim 12\%$ 0–14%) (Hückstädt et al., 2012; Valenzuela et al., 2018; Reisinger et al., 2016; Van Den Berg et al., 2021). The increase in δ^{15} N is unlikely to reflect higher trophic status (Hodum and Hobson, 2000) or coastal foraging (St John Glew et al., 2021), because the fatty acid distributions suggest high Antarctic krill contributions to the diet, which should introduce lower δ^{15} N than fish (Rau et al., 1992) and are associated with pelagic foraging (Brault et al., 2018). In zone Org-C, there could be potential for microbial degradation or enhanced guano inputs causing elevated δ^{15} N. However, we also note that high $\delta^{15}N$ are coincident with peak $C_{14:0}$ FA fluxes ~ 6400 cal. yrBP, suggesting foraging could have occurred in pelagic waters with high nitrate utilisation (cf. Studer et al., 2018), consistent with nutrient limitation in highly productive polynyas. The presence of Antarctic krill markers suggests foraging in an open-ocean polynya, such as the intermittent Maud Rise polynya (Fig. 1) (Jena and Pillai, 2020; Turner et al., 2020; Holland, 2001). Feeding at the Maud Rise polynya is possible as snow petrels are able to forage at long ranges > 700 km (Honan et al., 2025), although they preferentially feed in broken ice in proximity to their nesting site during chick-rearing (Wakefield et al., 2025). Further work is required to identify whether other records with elevated $\delta^{15}N$ can be identified, or to rule out an impact from guano or degradation on the unusual δ^{15} N values in zone Org-C, especially as low %N could indicate degradation. At present, we interpret the data from zone Org-C to reflect foraging in a MIZ situated in pelagic waters but with the potential for foraging over the continental shelf during intervals when the MIZ was situated closer to the coast.

4.2.2 Zone Org-B (5960–4320 cal. yr BP)

Between 5960–4320 cal. yr BP, we infer snow petrel foraging which is in a similar or slightly more productive MIZ than in zone Org-C due to elevated contributions from phytol. A mixed diet is inferred from intermediate contributions from $C_{14:0}$ (FA) and $C_{18:1(n-9)}$, from Antarctic krill and fish, respectively, with no change in diet compared to zone Org-C based on the fatty acid ratios $C_{16:0}/C_{14:0}$ and $C_{18:0}/C_{14:0}$ (Fig. 3). This mixed diet continues to indicate feeding both at the continental shelf edge and offshore. The main difference between zones Org-C and Org-B appear to be in the higher %N and sustained inputs of phytol, suggesting a more stable interval of higher productivity (and potentially better preservation) compared to the more variable zone Org-C. High accumulation rates in zone Org-B (Fig. 2) suggest frequent nest occupation during this zone, supported by elevated and sustained accumulation rates for the productivity marker (phytol) (Figs. 3 and 5) and inputs of potential guano-related elements (Fig. 4). Phytol is formed from chlorophyll a (Rontani and Volkman, 2003) and is brought into snow petrel diet through krill gut contents (Sargent and Falk-Petersen, 1981). As for zone Org-C, foraging in productive waters relatively proximal to the nest site could be explained either by access to foraging in coastal polynyas if the MIZ was situated further offshore, or by a MIZ relatively close to the continent e.g. if winter or spring sea-ice extents are relatively low, enabled in part by ice shelf fronts which were relatively stable during this period (Grieman et al., 2024). The variable but continued presence of Antarctic krill markers implies that there were several intervals where foraging occurred in a MIZ which was situated in pelagic waters between 5960 and 4320 cal. yr BP.

4.2.3 Zone Org-A (4320–1830 cal. yr BP)

We infer that between 4320 and 1830 cal. yr BP there was a shift towards a cooler, or neoglacial, phase which is characterised by more extensive sea ice. Our interpretation is based on the lower concentrations and fluxes in most of the organic proxies, aligning with sustained low accumulation rates in zone Org-A (Figs. 2–4). Although we observe no significant changes to diet according to the fatty acid ratios $C_{16:0}/C_{14:0}$ and $C_{18:0}/C_{14:0}$ (Fig. 3), the loss of phytol indicates very low primary productivity, and the loss of cholesterol and Cu suggests that contributions from Antarctic krill were also reduced. In zone Org-A we suggest that the low rates of nest occupation and reduction in Antarctic krill and productivity markers indicate limited accessibility to snow petrel prey from the Heimefrontfjella site, which is consistent with the development of a more extensive or more dense sea ice pack

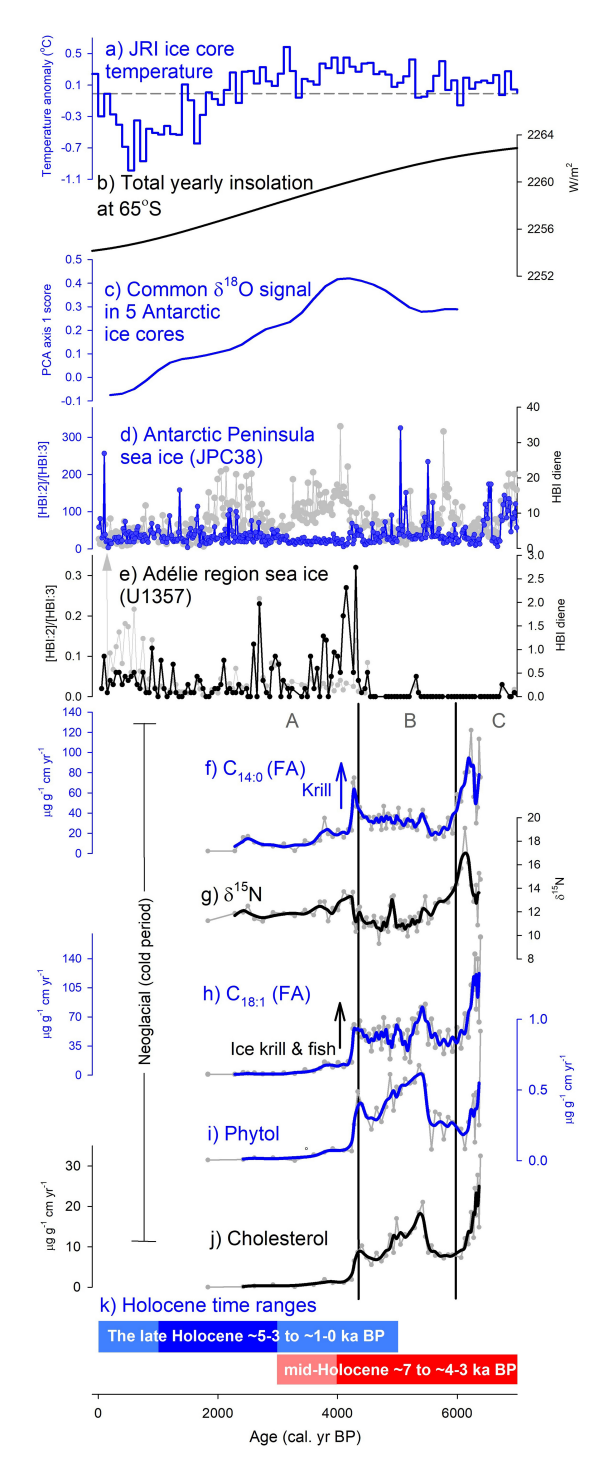


Figure 5. Summary plot comparing the marine and ice-core climate proxies (**a–e**) with 3012MUM2 geochemical proxy data (**f–j**). (**a**) James Ross Island (JRI) ice core temperature anomaly relative to 1961–1990 mean based on 100 year averages in Mulvaney et al. (2012); (**b**) Total yearly insolation at 65° S (Laskar et al., 2004); (**c**) Common δ^{18} O signal in 5 Antarctic ice cores, interpreted by PCA axis 1 scores from Hodgson and Bentley (2013) based on common and residual signals in five Antarctic δ^{18} O records; Vostok, Taylor Dome, EPICA Dome C, EPICA Dronning Maud Land and Dome Fuji (Masson-Delmotte et al., 2011); (**d**) Antarctic Peninsula sea ice from the ratio of highly-branched isoprenoid (HBI) diene to triene and HBI diene individually (core JPC38) (Barbara et al., 2016); (**e**) Adélie region sea ice from the ratio of HBI diene to triene and HBI diene individually (core U1257) (Ashley et al., 2021); (**f**) C_{14:0} (FA) flux as a krill maker; (**g**) nitrogen stable isotopes (δ^{15} N); (**h**) C_{18:1(n-9)} (FA) flux as an ice krill and fish marker; (**i**) phytol flux as a productivity marker; (**j**) cholesterol flux; and (**k**) Holocene time ranges for palaeoclimate periods from Crosta et al. (2022). Smooth lines are calculated from moving averages. Cluster boundaries (vertical black lines) are based on zones Org-A–C in Fig. 3.

in the north-east Weddell Sea which displaced the MIZ further offshore.

4.3 Coherence with other records of Holocene environmental change

Our records show associations between inference of past sea ice configurations made from our snow petrel stomach oil deposit and regional records of environmental change. For example, there are similarities and differences with records in the wider Weddell Sea region, likely due to the influence of the Weddell Gyre and atmospheric processes that determine sea ice configurations. Our interpretations of high productivity and krill between 6390 and 5960 cal. kyr BP (zone Org-C, Figs. 3 and 5), correspond with a relatively productive and an open-ocean (pelagic) type sea ice configuration from 7.2 cal. kyr BP at Herbert Sound and Croft Bay, in response to a wider regional mid-Holocene warming (e.g. core NBP0502-Site 2) (Totten et al., 2015). In the Firth of Tay (Fig. 1), this mid-Holocene climatic optimum spans 7800–6000 cal. yr BP (core NBP0602A) (Michalchuk et al., 2009) and 7750 and 6000 yr BP (cores NBP0602A-8B and NBP0703-JPC02) (Majewski and Anderson, 2009), and was attributed to seasonally-open marine conditions. Scotia Sea diatom records are also in phase with our results, with seasonally open water assemblages from 8300 to 2400 yr BP (core SS01) (Bak et al., 2007).

Our interpretation of zone Org-A having more sea ice corresponds with HBI records at the Vega Drift in JPC38, when interpreted carefully (Fig. 5d) (Barbara et al., 2016). Higher HBI diene levels in our deposit zone Org-A (4320–1830 cal. yr BP) correspond to increased sea ice cover. The fact that HBI:2 / HBI:3 ratios vary and are low in zone Org-A are probably due to limitations of the proxy and the issue of normalization, linked with variable pelagic productivity. At Bransfield Strait (core D1–7) persistent sea ice is observed between 5.8 and 3.8 ka BP (core ANT28/D1–7) (Nie et al., 2022).

The neoglacial, sea-ice expansion and cooling phase suggested by zone Org-A is coherent with a sediment record on the Firth of Tay (core NBP0602A-8B and NBP0703-JPC02) which shows cooling from ~3500 yrBP based on foraminifera (Majewski and Anderson, 2009). At Perseverance Drift, the warm interval persists longer than in our deposit, with high abundance of the foraminifera *Globocassidulina* spp. between 3400 and 1800 yrBP indicating incursions of Weddell Sea Transitional Water and a period of "freshening" consistent with open-marine or seasonally open marine conditions (Kyrmanidou et al., 2018) (cores JKC36 and JPC36), indicative of cooling.

The boundary between zone Org-B and A (4320 cal. yr BP) aligns with the transition to neoglacial conditions (e.g. Crosta et al., 2022). This mid-Holocene neoglacial is consistent with the James Ross Island (JRI) ice core temperature decline (Fig. 5a) (Mulvaney et al., 2012) and decreasing δ^{18} O sig-

nal in 5 Antarctic ice cores (Hodgson and Bentley, 2013; Masson-Delmotte et al., 2011) (Fig. 5c). We find that the onset of the neoglacial is remarkably in phase with a switch in sea ice biomarkers (both HBI diene and (HBI : 2/HBI : 3) ratio) indicative of more sea ice in the distant Adélie region in core U1357 (Ashley et al., 2021) (Fig. 5e). A marked transition is also seen in South Atlantic cores (Hodell et al., 2001) where IRD (as % lithics) increase markedly from \sim 5 ka BP suggesting cooling waters (together with concomitant changes in diatoms SST index and δ^{18} O on diatoms) which have been linked to the arrival of more sea ice from the Weddell Sea region (core TTN057-13-PC4). Total yearly insolation (e.g. at 65° S) features an ongoing decline during this period (Fig. 5b) but is unlikely to be the sole driver of the neoglacial (Divine et al., 2010; Renssen et al., 2005).

5 Conclusions

Analyses of accumulation rates and a range of biomarkers in a snow petrel stomach-oil deposit from the Heimefrontfjella Range have been used to infer sea ice conditions in the foraging area in the northeastern Weddell Sea over the Holocene. The record has three significant zones. In the first zone between 6390 and 5960 cal. yr BP, high stomach oil accumulation rates and high concentrations of both fish and krill fatty acids suggest easy access to productive foraging grounds. This is consistent with foraging both at the continental shelf in the MIZ and offshore. In the second zone, between 5960 and 4320 cal. yr BP productivity remained high but there was evidence of a more mixed diet suggesting foraging both at the continental shelf edge and in open water, with high productivity due to summer sea ice retreat reaching the shelf edge more frequently. In the third stage, between 4320 and 1830 cal. yr BP low stomach oil accumulation rates and reductions productivity markers indicate that increased sea ice conditions consistent with the transition to neoglacial conditions seen in a range of records from the northwestern Weddell Sea (Barbara et al., 2016; Nie et al., 2022), from ice records on the Antarctic continent (Hodgson and Bentley, 2013), and changes elsewhere in the wider Antarctic region including Adélie Land (Ashley et al., 2021) and the South Atlantic (Hodell et al., 2001; Divine et al., 2010). This study has also shown, for the first time, the utility of phytol and cholesterol for tracking past snow petrel diet and thus interpretation of environmental conditions in their foraging areas.

Data availability. All data presented within this manuscript is available in the PANGAEA data repository at https://doi.org/10.1594/PANGAEA.980519 (Stevenson et al., 2025).

Supplement. The supplement related to this article is available online at https://doi.org/10.5194/cp-21-2465-2025-supplement.

Author contributions. ELM obtained main funding. MAS, DRG, NT, CL, AG, and ELM carried out the laboratory work and data analysis. MJB and DAH collected samples from Antarctica. MAS prepared the initial paper and revised the manuscript during the review process, discussing interpretations with ELM, MJB and DAH.

Competing interests. At least one of the (co-)authors is a member of the editorial board of *Climate of the Past*. The peer-review process was guided by an independent editor, and the authors also have no other competing interests to declare.

Disclaimer. Publisher's note: Copernicus Publications remains neutral with regard to jurisdictional claims made in the text, published maps, institutional affiliations, or any other geographical representation in this paper. While Copernicus Publications makes every effort to include appropriate place names, the final responsibility lies with the authors. Views expressed in the text are those of the authors and do not necessarily reflect the views of the publisher.

Acknowledgements. Our thanks are given to the BAS field operations staff and pilots, Andy Hein and Al Davies for assistance with field sampling and Kerry A. Strong, Martin D. West and Amanda Hayton for laboratory assistance. We also thank Helen Mackay for advice and assistance regarding the interpretation of sterols and stanols, Ewan Wakefield for insights on snow petrel feeding ranges and seasonality, James Grecian for discussion of Southern Ocean/Weddell Sea species distribution references and Richard Staff for assistance with OxCal. We thank an anonymous reviewer and Xavier Crosta for helpful comments on the manuscript during the review process.

Financial support. This research has been supported by the H2020 European Research Council (ANTSIE, grant no. 864637), the Leverhulme Trust (Philip Leverhulme Research Leadership Award, grant no. RL-2019-023), and the Natural Environment Research Council, British Antarctic Survey (grant no. NE/K003674/1).

Review statement. This paper was edited by Alessio Rovere and reviewed by Xavier Crosta and one anonymous referee.

References

Ai, X. E., Studer, A. S., Sigman, D. M., Martínez-García, A., Fripiat, F., Thöle, L. M., Michel, E., Gottschalk, J., Arnold, L., Moretti, S., Schmitt, M., Oleynik, S., Jaccard, S. L., and Haug, G. H.: Southern Ocean upwelling, Earth's obliquity, and glacial-

- interglacial atmospheric CO₂ change, Science, 370, 1348–1352, https://doi.org/10.1126/science.abd2115, 2020.
- Ainley, D. G., O'Connor, E. F., and Boekelheide, R. J.: The Marine Ecology of Birds in the Ross Sea, Antarctica, Ornithological Monographs, 32, iii-97, https://doi.org/10.2307/40166773, 1984.
- Ainley, D. G., Jacobs, S. S., Ribic, C. A., and Gaffney, I.: Seabird distribution and oceanic features of the Amundsen and southern Bellingshausen seas, Antarctic Science, 10, 111–123, https://doi.org/10.1017/S0954102098000169, 1998.
- Ainley, D. G., Hobson, K. A., Crosta, X., Rau, G. H., Wassenaar, L. I., and Augustinus, P. C.: Holocene variation in the Antarctic coastal food web: linking δD and $\delta^{13}C$ in snow petrel diet and marine sediments, Marine Ecology Progress Series, 306, 31–40, 2006.
- Arrigo, K. R., Lubin, D., van Dijken, G. L., Holm-Hansen, O., and Morrow, E.: Impact of a deep ozone hole on Southern Ocean primary production, Journal of Geophysical Research-Oceans, 108, https://doi.org/10.1029/2001JC001226, 2003.
- Ashley, K. E., McKay, R., Etourneau, J., Jimenez-Espejo, F. J., Condron, A., Albot, A., Crosta, X., Riesselman, C., Seki, O., Massé, G., Golledge, N. R., Gasson, E., Lowry, D. P., Barrand, N. E., Johnson, K., Bertler, N., Escutia, C., Dunbar, R., and Bendle, J. A.: Mid-Holocene Antarctic sea-ice increase driven by marine ice sheet retreat, Clim. Past, 17, 1–19, https://doi.org/10.5194/cp-17-1-2021, 2021.
- Bak, Y.-S., Yoo, K.-C., Yoon, H. I., Lee, J.-D., and Yun, H.: Diatom evidence for Holocene paleoclimatic change in the South Scotia Sea, West Antarctica, Geosciences Journal, 11, 11–22, https://doi.org/10.1007/BF02910377, 2007.
- Barbara, L., Crosta, X., Massé, G., and Ther, O.: Deglacial environments in eastern Prydz Bay, East Antarctica, Quaternary Science Reviews, 29, 2731–2740, https://doi.org/10.1016/j.quascirev.2010.06.027, 2010.
- Barbara, L., Crosta, X., Schmidt, S., and Massé, G.: Diatoms and biomarkers evidence for major changes in sea ice conditions prior the instrumental period in Antarctic Peninsula, Quaternary Science Reviews, 79, 99–110, https://doi.org/10.1016/j.quascirev.2013.07.021, 2013.
- Barbara, L., Crosta, X., Leventer, A., Schmidt, S., Etourneau, J., Domack, E., and Massé, G.: Environmental responses of the Northeast Antarctic Peninsula to the Holocene climate variability, Paleoceanography, 31, 131–147, https://doi.org/10.1002/2015PA002785, 2016.
- Bennett, K. D.: Determination of the number of zones in a biostratigraphical sequence, New Phytologist, 132, 155–170, https://doi.org/10.1111/j.1469-8137.1996.tb04521.x, 1996.
- Bentley, M. J., Ó Cofaigh, C., Anderson, J. B., Conway, H., Davies, B., Graham, A. G. C., Hillenbrand, C.-D., Hodgson, D. A., Jamieson, S. S. R., Larter, R. D., Mackintosh, A., Smith, J. A., Verleyen, E., Ackert, R. P., Bart, P. J., Berg, S., Brunstein, D., Canals, M., Colhoun, E. A., Crosta, X., Dickens, W. A., Domack, E., Dowdeswell, J. A., Dunbar, R., Ehrmann, W., Evans, J., Favier, V., Fink, D., Fogwill, C. J., Glasser, N. F., Gohl, K., Golledge, N. R., Goodwin, I., Gore, D. B., Greenwood, S. L., Hall, B. L., Hall, K., Hedding, D. W., Hein, A. S., Hocking, E. P., Jakobsson, M., Johnson, J. S., Jomelli, V., Jones, R. S., Klages, J. P., Kristoffersen, Y., Kuhn, G., Leventer, A., Licht, K., Lilly, K., Lindow, J., Livingstone, S. J., Massé, G., McGlone, M. S., McKay, R. M., Melles, M., Miura, H., Mulvaney, R.,

- Nel, W., Nitsche, F. O., O'Brien, P. E., Post, A. L., Roberts, S. J., Saunders, K. M., Selkirk, P. M., Simms, A. R., Spiegel, C., Stolldorf, T. D., Sugden, D. E., van der Putten, N., van Ommen, T., Verfaillie, D., Vyverman, W., Wagner, B., White, D. A., Witus, A. E., and Zwartz, D.: A community-based geological reconstruction of Antarctic Ice Sheet deglaciation since the Last Glacial Maximum, Quaternary Science Reviews, 100, 1–9, https://doi.org/10.1016/j.quascirev.2014.06.025, 2014.
- Berg, S., Melles, M., Hermichen, W.-D., McClymont, E. L., Bentley, M. J., Hodgson, D. A., and Kuhn, G.: Evaluation of Mumiyo Deposits From East Antarctica as Archives for the Late Quaternary Environmental and Climatic History, Geochemistry Geophysics Geosystems, 20, 260–276, https://doi.org/10.1029/2018GC008054, 2019.
- Berg, S., Emmerson, L., Heim, C., Buchta, E., Fromm, T., Glaser, B., Hermichen, W.-D., Rethemeyer, J., Southwell, C., Wand, U., Zech, M., and Melles, M.: Reconstructing the Paleo-Ecological Diet of Snow Petrels (*Pagodroma nivea*) From Modern Samples and Fossil Deposits: Implications for Southern Ocean Paleoenvironmental Reconstructions, Journal of Geophysical Research-Biogeosciences, 128, e2023JG007454, https://doi.org/10.1029/2023JG007454, 2023.
- Bianchi, C. and Gersonde, R.: Climate evolution at the last deglaciation: the role of the Southern Ocean, Earth and Planetary Science Letters, 228, 407–424, https://doi.org/10.1016/j.epsl.2004.10.003, 2004.
- Björck, S., Hjort, C., Ingólfsson, O., and Skog, G.: Radiocarbon dates from the Antarctic Peninsula – problems and potential, in: Radiocarbon Dating: Recent Applications and Future Potential, edited by: Lowe, J. J., Quaternary Research Association, Cambridge, 55–65, ISSN 0963-1895, 1991.
- Bokhorst, S., Huiskes, A., Convey, P., and Aerts, R.: External nutrient inputs into terrestrial ecosystems of the Falkland Islands and the Maritime Antarctic region, Polar Biology, 30, 1315–1321, https://doi.org/10.1007/s00300-007-0292-0, 2007.
- Brandon, M. A., Cottier, F. R., and Nilsen, F.: Sea Ice and Oceanography, in: Sea Ice, 2nd edn., edited by: Thomas, D. N. and Dieckmann, G. S., Wiley-Blackwell, Chichester, United Kingdom, 79–111, ISBN 978-1-4051-8580-6, 2010.
- Brault, E. K., Koch, P. L., McMahon, K. W., Broach, K. H., Rosenfield, A. P., Sauthoff, W., Loeb, V. J., Arrigo, K. R., and Smith Jr., W, O.: Carbon and nitrogen zooplankton isoscapes in West Antarctica reflect oceanographic transitions, Marine Ecology Progress Series, 593, 29–45, 2018.
- Bridges, C.: Structure and function of krill (*Euphasia superba*) hemocyanin-adaption to life at low temperature, Structure and function of invertebrate respiratory proteins Life, Chemistry Reports, 1, 353–356, 1983.
- Bronk Ramsey, C.: Bayesian Analysis of Radiocarbon Dates, Radiocarbon, 51, 337–360, https://doi.org/10.1017/S0033822200033865, 2009.
- Castro, M. F., Neves, J. C. L., Francelino, M. R., Schaefer, C. E. G. R., and Oliveira, T. S.: Seabirds enrich Antarctic soil with trace metals in organic fractions, Science of the Total Environment, 785, 147271, https://doi.org/10.1016/j.scitotenv.2021.147271, 2021.
- Chen, T., Robinson, L. F., Li, T., Burke, A., Zhang, X., Stewart, J. A., White, N. J., and Knowles, T. D. J.: Radiocarbon evidence for the stability of polar ocean overturning during the Holocene, Na-

- ture Geoscience, 16, 631–636, https://doi.org/10.1038/s41561-023-01214-2, 2023.
- Cheng, W., Sun, L., Kimpe, L. E., Mallory, M. L., Smol, J. P., Gallant, L. R., Li, J., and Blais, J. M.: Sterols and Stanols Preserved in Pond Sediments Track Seabird Biovectors in a High Arctic Environment, Environmental Science & Technology, 50, 9351–9360, https://doi.org/10.1021/acs.est.6b02767, 2016.
- Clarke, A.: Lipid Content and Composition of Antarctic Krill, Euphausia Superba Dana, Journal of Crustacean Biology, 4, 285–294, https://doi.org/10.1163/1937240x84x00660, 1984.
- Collins, M., Knutti, R., Arblaster, J., Dufresne, J.-L., Fichefet, T., Friedlingstein, P., Gao, X., Gutowski, W. J., Johns, T., and Krinner, G.: Long-term climate change: projections, commitments and irreversibility, in: Climate Change 2013–The Physical Science Basis: Contribution of Working Group I to the Fifth Assessment Report of the Intergovernmental Panel on Climate Change, Cambridge University Press, 1029–1136, ISBN 978-1-107-05799-1, 2013.
- Comiso, J. C. and Gordon, A. L.: Recurring polynyas over the Cosmonaut Sea and the Maud Rise, Journal of Geophysical Research-Oceans, 92, 2819–2833, https://doi.org/10.1029/JC092iC03p02819, 1987.
- Connan, M., Mayzaud, P., Trouvé, C., Barbraud, C., and Cherel, Y.: Interannual dietary changes and demographic consequences in breeding blue petrels from Kerguelen Islands, Marine Ecology Progress Series, 373, 123–135, 2008.
- Cripps, G. C., Watkins, J. L., Hill, H. J., and Atkinson, A.: Fatty acid content of Antarctic krill Euphausia superba at South Georgia related to regional populations and variations in diet, Marine Ecology Progress Series, 181, 177–188, 1999.
- Crosta, X., Denis, D., and Ther, O.: Sea ice seasonality during the Holocene, Adélie Land, East Antarctica, Marine Micropaleontology, 66, 222–232, https://doi.org/10.1016/j.marmicro.2007.10.001, 2008.
- Crosta, X., Etourneau, J., Orme, L. C., Dalaiden, Q., Campagne, P., Swingedouw, D., Goosse, H., Massé, G., Miettinen, A., McKay, R. M., Dunbar, R. B., Escutia, C., and Ikehara, M.: Multidecadal trends in Antarctic sea-ice extent driven by ENSO–SAM over the last 2,000 years, Nature Geoscience, 14, 156–160, https://doi.org/10.1038/s41561-021-00697-1, 2021.
- Crosta, X., Kohfeld, K. E., Bostock, H. C., Chadwick, M., Du Vivier, A., Esper, O., Etourneau, J., Jones, J., Leventer, A., Müller, J., Rhodes, R. H., Allen, C. S., Ghadi, P., Lamping, N., Lange, C. B., Lawler, K.-A., Lund, D., Marzocchi, A., Meissner, K. J., Menviel, L., Nair, A., Patterson, M., Pike, J., Prebble, J. G., Riesselman, C., Sadatzki, H., Sime, L. C., Shukla, S. K., Thöle, L., Vorrath, M.-E., Xiao, W., and Yang, J.: Antarctic sea ice over the past 130 000 years Part 1: a review of what proxy records tell us, Clim. Past, 18, 1729–1756, https://doi.org/10.5194/cp-18-1729-2022, 2022.
- Delord, K., Pinet, P., Pinaud, D., Barbraud, C., De Grissac, S., Lewden, A., Cherel, Y., and Weimerskirch, H.: Species-specific foraging strategies and segregation mechanisms of sympatric Antarctic fulmarine petrels throughout the annual cycle, Ibis, 158, 569–586, https://doi.org/10.1111/ibi.12365, 2016.
- Denis, D., Crosta, X., Barbara, L., Massé, G., Renssen, H., Ther, O., and Giraudeau, J.: Sea ice and wind variability during the Holocene in East Antarctica: insight on middle-high lat-

- itude coupling, Quaternary Science Reviews, 29, 3709–3719, https://doi.org/10.1016/j.quascirev.2010.08.007, 2010.
- Divine, D. V., Koç, N., Isaksson, E., Nielsen, S., Crosta, X., and Godtliebsen, F.: Holocene Antarctic climate variability from ice and marine sediment cores: Insights on ocean–atmosphere interaction, Quaternary Science Reviews, 29, 303–312, https://doi.org/10.1016/j.quascirev.2009.11.012, 2010.
- Duda, M. P., Hargan, K. E., Michelutti, N., Blais, J. M., Grooms, C., Gilchrist, H. G., Mallory, M. L., Robertson, G. J., and Smol, J. P.: Reconstructing Long-Term Changes in Avian Populations Using Lake Sediments: Opening a Window Onto the Past, Frontiers in Ecology and Evolution, 9, https://doi.org/10.3389/fevo.2021.698175, 2021.
- Eayrs, C., Li, X., Raphael, M. N., and Holland, D. M.: Rapid decline in Antarctic sea ice in recent years hints at future change, Nature Geoscience, 14, 460–464, https://doi.org/10.1038/s41561-021-00768-3, 2021.
- Etourneau, J., Collins, L. G., Willmott, V., Kim, J.-H., Barbara, L., Leventer, A., Schouten, S., Sinninghe Damsté, J. S., Bianchini, A., Klein, V., Crosta, X., and Massé, G.: Holocene climate variations in the western Antarctic Peninsula: evidence for sea ice extent predominantly controlled by changes in insolation and ENSO variability, Clim. Past, 9, 1431–1446, https://doi.org/10.5194/cp-9-1431-2013, 2013.
- Ferrari, R., Jansen, M. F., Adkins, J. F., Burke, A., Stewart, A. L., and Thompson, A. F.: Antarctic sea ice control on ocean circulation in present and glacial climates, Proceedings of the National Academy of Sciences USA, 111, 8753–8758, https://doi.org/10.1073/pnas.1323922111, 2014.
- Fetterer, F., Knowles, K., Meier, W., Savoie, M., and Windnagel, A.: Sea Ice Index. (G02135, Version 3), NSIDC: National Snow and Ice Data Center [data set], Boulder, Colorado, USA, https://doi.org/10.7265/N5K072F8, 2017.
- Freer, J. J., Tarling, G. A., Collins, M. A., Partridge, J. C., and Genner, M. J.: Predicting future distributions of lanternfish, a significant ecological resource within the Southern Ocean, Diversity and Distributions, 25, 1259–1272, https://doi.org/10.1111/ddi.12934, 2019.
- Gilbert, E. and Holmes, C.: 2023's Antarctic sea ice extent is the lowest on record, Weather, 79, 46–51, https://doi.org/10.1002/wea.4518, 2024.
- Grieman, M. M., Nehrbass-Ahles, C., Hoffmann, H. M., Bauska, T. K., King, A. C. F., Mulvaney, R., Rhodes, R. H., Rowell, I. F., Thomas, E. R., and Wolff, E. W.: Abrupt Holocene ice loss due to thinning and ungrounding in the Weddell Sea Embayment, Nature Geoscience, 17, 227–232, https://doi.org/10.1038/s41561-024-01375-8, 2024.
- Gupta, M., Regan, H., Koo, Y., Chua, S. M. T., Li, X., and Heil, P.: Inferring the seasonality of sea ice floes in the Weddell Sea using ICESat-2, The Cryosphere, 19, 1241–1257, https://doi.org/10.5194/tc-19-1241-2025, 2025.
- Heaton, T. J., Köhler, P., Butzin, M., Bard, E., Reimer, R. W., Austin, W. E. N., Bronk Ramsey, C., Grootes, P. M., Hughen, K. A., Kromer, B., Reimer, P. J., Adkins, J., Burke, A., Cook, M. S., Olsen, J., and Skinner, L. C.: Marine20 – The Marine Radiocarbon Age Calibration Curve (0–55,000 cal BP), Radiocarbon, 62, 779–820, https://doi.org/10.1017/RDC.2020.68, 2020.
- Hillenbrand, C.-D., Smith, J. A., Hodell, D. A., Greaves, M., Poole, C. R., Kender, S., Williams, M., Andersen, T. J., Jer-

- nas, P. E., Elderfield, H., Klages, J. P., Roberts, S. J., Gohl, K., Larter, R. D., and Kuhn, G.: West Antarctic Ice Sheet retreat driven by Holocene warm water incursions, Nature, 547, 43–48, https://doi.org/10.1038/nature22995, 2017.
- Hiller, A., Wand, U., Kämpf, H., and Stackebrandt, W.: Occupation of the Antarctic continent by petrels during the past 35 000 years: Inferences from a ¹⁴C study of stomach oil deposits, Polar Biology, 9, 69–77, https://doi.org/10.1007/BF00442032, 1988.
- Hodell, D. A., Kanfoush, S. L., Shemesh, A., Crosta, X., Charles, C. D., and Guilderson, T. P.: Abrupt Cooling of Antarctic Surface Waters and Sea Ice Expansion in the South Atlantic Sector of the Southern Ocean at 5000 cal yr B.P., Quaternary Research, 56, 191–198, https://doi.org/10.1006/qres.2001.2252, 2001.
- Hodgson, D. A. and Bentley, M. J.: Lake highstands in the Pensacola Mountains and Shackleton Range 4300– 2250 cal. yr BP: Evidence of a warm climate anomaly in the interior of Antarctica, Holocene, 23, 388–397, https://doi.org/10.1177/0959683612460790, 2013.
- Hodum, P. J. and Hobson, K. A.: Trophic relationships among Antarctic fulmarine petrels: insights into dietary overlap and chick provisioning strategies inferred from stable-isotope (δ^{15} N and δ^{13} C) analyses, Marine Ecology Progress Series, 198, 273–281, 2000.
- Holland, D. M.: Explaining the Weddell Polynya–a Large Ocean Eddy Shed at Maud Rise, Science, 292, 1697–1700, https://doi.org/10.1126/science.1059322, 2001.
- Honan, E. M., Wakefield, E. D., Phillips, R. A., Grecian, W. J., Prince, S., Robert, H., Descamps, S., Rix, A., Hoelzel, A. R., and McClymont, E. L.: The foraging distribution and habitat use of chick-rearing snow petrels from two colonies in Dronning Maud Land, Antarctica, Marine Biology, 172, 109, https://doi.org/10.1007/s00227-025-04657-w, 2025.
- Hückstädt, L. A., Koch, P. L., McDonald, B. I., Goebel, M. E., Crocker, D. E., and Costa, D. P.: Stable isotope analyses reveal individual variability in the trophic ecology of a top marine predator, the southern elephant seal, Oecologia, 169, 395–406, https://doi.org/10.1007/s00442-011-2202-y, 2012.
- Hutchings, J. K., Heil, P., Steer, A., and Hibler III, W. D.: Subsynoptic scale spatial variability of sea ice deformation in the western Weddell Sea during early summer, Journal of Geophysical Research-Oceans, 117, https://doi.org/10.1029/2011JC006961, 2012.
- Imber, M. J.: The Origin of Petrel Stomach Oils: A Review, Condor, 78, 366–369, https://doi.org/10.2307/1367697, 1976.
- Ionita, M.: Large-scale drivers of the exceptionally low winter Antarctic sea ice extent in 2023, Frontiers in Earth Science, 12, https://doi.org/10.3389/feart.2024.1333706, 2024.
- Jena, B. and Pillai, A. N.: Satellite observations of unprecedented phytoplankton blooms in the Maud Rise polynya, Southern Ocean, The Cryosphere, 14, 1385–1398, https://doi.org/10.5194/tc-14-1385-2020, 2020.
- Johnson, J. S., Nichols, K. A., Goehring, B. M., Balco, G., and Schaefer, J. M.: Abrupt mid-Holocene ice loss in the western Weddell Sea Embayment of Antarctica, Earth and Planetary Science Letters, 518, 127–135, https://doi.org/10.1016/j.epsl.2019.05.002, 2019.
- Johnson, K. M., McKay, R. M., Etourneau, J., Jiménez-Espejo, F. J., Albot, A., Riesselman, C. R., Bertler, N. A. N., Horgan, H. J., Crosta, X., Bendle, J., Ashley, K. E., Yamane, M.,

- Yokoyama, Y., Pekar, S. F., Escutia, C., and Dunbar, R. B.: Sensitivity of Holocene East Antarctic productivity to subdecadal variability set by sea ice, Nature Geoscience, 14, 762–768, https://doi.org/10.1038/s41561-021-00816-y, 2021.
- Ju, S.-J. and Harvey, H. R.: Lipids as markers of nutritional condition and diet in the Antarctic krill Euphausia superba and Euphausia crystallorophias during austral winter, Deep Sea Research Part II-Topical Studies in Oceanography, 51, 2199–2214, https://doi.org/10.1016/j.dsr2.2004.08.004, 2004.
- Juckes, L.: The geology of north-eastern Heimefrontfjella, Dronning Maud Land, British Antarctic Survey, ISBN 0856650145, https://nora.nerc.ac.uk/id/eprint/509222 (last access: 15 October 2025), 1972.
- Juggins, S.: rioja: Analysis of Quaternary Science Data, R package version 0.9-26, University of Newcastle upon Tyne, Newcastle upon Tyne, https://cran.r-project.org/web/packages/rioja/rioja.pdf (last access: 15 October 2025), 2020.
- Kemeny, P. C., Kast, E. R., Hain, M. P., Fawcett, S. E., Fripiat, F., Studer, A. S., Martínez-García, A., Haug, G. H., and Sigman, D. M.: A Seasonal Model of Nitrogen Isotopes in the Ice Age Antarctic Zone: Support for Weakening of the Southern Ocean Upper Overturning Cell, Paleoceanography and Paleoclimatology, 33, 1453–1471, https://doi.org/10.1029/2018PA003478, 2018.
- Kyrmanidou, A., Vadman, K. J., Ishman, S. E., Leventer, A., Brachfeld, S., Domack, E. W., and Wellner, J. S.: Late Holocene oceanographic and climatic variability recorded by the Perseverance Drift, northwestern Weddell Sea, based on benthic foraminifera and diatoms, Marine Micropaleontology, 141, 10–22, https://doi.org/10.1016/j.marmicro.2018.03.001, 2018.
- Laskar, J., Robutel, P., Joutel, F., Gastineau, M., Correia, A. C. M., and Levrard, B.: A long-term numerical solution for the insolation quantities of the Earth, A&A, 428, 261–285, 2004.
- Lewis, R. W.: Studies of the glyceryl ethers of the stomach oil of Leach's petrel *Oceanodroma leucorhoa* (Viellot), Comparative Biochemistry and Physiology, 19, 363–377, https://doi.org/10.1016/0010-406X(66)90147-2, 1966.
- Lewis, R. W.: Studies on the stomach oils of marine animals II. Oils of some procellariiform birds, Comparative Biochemistry and Physiology, 31, 725–731, https://doi.org/10.1016/0010-406X(69)92072-6, 1969.
- Liu, S., Liu, Y., Teschke, K., Hindell, M. A., Downey, R., Woods, B., Kang, B., Ma, S., Zhang, C., Li, J., Ye, Z., Sun, P., He, J., and Tian, Y.: Incorporating mesopelagic fish into the evaluation of conservation areas for marine living resources under climate change scenarios, Marine Life Science & Technology, 6, 68–83, https://doi.org/10.1007/s42995-023-00188-9, 2024.
- Liu, X., Sun, L., Xie, Z., Yin, X., and Wang, Y.: A 1300-year Record of Penguin Populations at Ardley Island in the Antarctic, as Deduced from the Geochemical Data in the Ornithogenic Lake Sediments, Arctic Antarctic and Alpine Research, 37, 490–498, https://doi.org/10.1657/1523-0430(2005)037[0490:AYROPP]2.0.CO;2, 2005.
- Macko, S. A. and Estep, M. L. F.: Microbial alteration of stable nitrogen and carbon isotopic compositions of organic matter, Organic Geochemistry, 6, 787–790, https://doi.org/10.1016/0146-6380(84)90100-1, 1984.
- Majewski, W. and Anderson, J. B.: Holocene foraminiferal assemblages from Firth of Tay, Antarctic Peninsula: Paleocli-

- mate implications, Marine Micropaleontology, 73, 135–147, https://doi.org/10.1016/j.marmicro.2009.08.003, 2009.
- Masson-Delmotte, V., Buiron, D., Ekaykin, A., Frezzotti, M., Gallée, H., Jouzel, J., Krinner, G., Landais, A., Motoyama, H., Oerter, H., Pol, K., Pollard, D., Ritz, C., Schlosser, E., Sime, L. C., Sodemann, H., Stenni, B., Uemura, R., and Vimeux, F.: A comparison of the present and last interglacial periods in six Antarctic ice cores, Clim. Past, 7, 397–423, https://doi.org/10.5194/cp-7-397-2011, 2011.
- McBride, M. M., Schram Stokke, O., Renner, A. H. H., Krafft, B. A., Bergstad, O. A., Biuw, M., Lowther, A. D., and Stiansen, J. E.: Antarctic krill Euphausia superba: spatial distribution, abundance, and management of fisheries in a changing climate, Marine Ecology Progress Series, 668, 185–214, 2021.
- McClymont, E. L., Bentley, M. J., Hodgson, D. A., Spencer-Jones, C. L., Wardley, T., West, M. D., Croudace, I. W., Berg, S., Gröcke, D. R., Kuhn, G., Jamieson, S. S. R., Sime, L., and Phillips, R. A.: Summer sea-ice variability on the Antarctic margin during the last glacial period reconstructed from snow petrel (*Pagodroma nivea*) stomach-oil deposits, Clim. Past, 18, 381–403, https://doi.org/10.5194/cp-18-381-2022, 2022.
- Mezgec, K., Stenni, B., Crosta, X., Masson-Delmotte, V., Baroni, C., Braida, M., Ciardini, V., Colizza, E., Melis, R., Salvatore, M. C., Severi, M., Scarchilli, C., Traversi, R., Udisti, R., and Frezzotti, M.: Holocene sea ice variability driven by wind and polynya efficiency in the Ross Sea, Nature Communications, 8, 1334, https://doi.org/10.1038/s41467-017-01455-x, 2017.
- Michalchuk, B. R., Anderson, J. B., Wellner, J. S., Manley, P. L., Majewski, W., and Bohaty, S.: Holocene climate and glacial history of the northeastern Antarctic Peninsula: the marine sedimentary record from a long SHALDRIL core, Quaternary Science Reviews, 28, 3049–3065, https://doi.org/10.1016/j.quascirev.2009.08.012, 2009.
- Mulvaney, R., Abram, N. J., Hindmarsh, R. C. A., Arrowsmith, C., Fleet, L., Triest, J., Sime, L. C., Alemany, O., and Foord, S.: Recent Antarctic Peninsula warming relative to Holocene climate and ice-shelf history, Nature, 489, 141–144, https://doi.org/10.1038/nature11391, 2012.
- Nichols, K. A., Goehring, B. M., Balco, G., Johnson, J. S., Hein, A. S., and Todd, C.: New Last Glacial Maximum ice thickness constraints for the Weddell Sea Embayment, Antarctica, The Cryosphere, 13, 2935–2951, https://doi.org/10.5194/tc-13-2935-2019, 2019.
- Nie, S., Xiao, W., and Wang, R.: Mid-Late Holocene climate variabilities in the Bransfield Strait, Antarctic Peninsula driven by insolation and ENSO activities, Palaeogeography Palaeoclimatology Palaeoecology, 601, 111140, https://doi.org/10.1016/j.palaeo.2022.111140, 2022.
- Nielsen, S. H. H., Koç, N. n., and Crosta, X.: Holocene climate in the Atlantic sector of the Southern Ocean: Controlled by insolation or oceanic circulation?, Geology, 32, 317–320, https://doi.org/10.1130/g20334.1, 2004.
- Nielsen, S. H. H., Hodell, D. A., Kamenov, G., Guilderson, T., and Perfit, M. R.: Origin and significance of ice-rafted detritus in the Atlantic sector of the Southern Ocean, Geochemistry Geophysics Geosystems, 8, https://doi.org/10.1029/2007GC001618, 2007.
- National Snow and Ice Data Center (NSIDC): Antarctic sea ice at near-record-low maximum extent for 2024, NSIDC [News Release, 3 October

- 2024], https://nsidc.org/news-analyses/news-stories/antarctic-sea-ice-near-record-low-maximum-extent-2024 (last access: 13 November 2025), 2024.
- Peck, V. L., Allen, C. S., Kender, S., McClymont, E. L., and Hodgson, D. A.: Oceanographic variability on the West Antarctic Peninsula during the Holocene and the influence of upper circumpolar deep water, Quaternary Science Reviews, 119, 54–65, https://doi.org/10.1016/j.quascirev.2015.04.002, 2015.
- Purich, A. and Doddridge, E. W.: Record low Antarctic sea ice coverage indicates a new sea ice state, Communications Earth & Environment, 4, 314, https://doi.org/10.1038/s43247-023-00961-9, 2023.
- Ran, Q., Duan, M., Wang, P., Ye, Z., Mou, J., Wang, X., Tian, Y., Zhang, C., Qiao, H., and Zhang, J.: Predicting the current habitat suitability and future habitat changes of Antarctic jonasfish Notolepis coatsorum in the Southern Ocean, Deep Sea Research Part II-Topical Studies in Oceanography, 199, 105077, https://doi.org/10.1016/j.dsr2.2022.105077, 2022.
- Rau, G. H., Ainley, D. G., Bengtson, J. L., Torres, J. J., and Hopkins, T. L.: ¹⁵N/¹⁴N and ¹³C/¹²C in Weddell Sea birds, seals, and fish: implications for diet and trophic structure, Marine Ecology Progress Series, 84, 1–8, 1992.
- Reisinger, R. R., Gröcke, D. R., Lübcker, N., McClymont, E. L., Hoelzel, A. R., and de Bruyn, P. J. N.: Variation in the diet of killer whales Orcinus orca at Marion Island, Southern Ocean, Marine Ecology Progress Series, 549, 263–274, 2016.
- Renssen, H., Goosse, H., Fichefet, T., Masson-Delmotte, V., and Koç, N.: Holocene climate evolution in the high-latitude Southern Hemisphere simulated by a coupled atmospheresea ice-ocean-vegetation model, Holocene, 15, 951–964, https://doi.org/10.1191/0959683605hl869ra, 2005.
- Rignot, E., Mouginot, J., and Scheuchl, B.: MEaSUREs Grounding Zone of the Antarctic Ice Sheet, Version 1, [2018], NASA National Snow and Ice Data Center Distributed Active Archive Center [data set], Boulder, Colorado, USA, https://doi.org/10.5067/HGLT8XB480E4, 2022.
- Roberts, S. J., Monien, P., Foster, L. C., Loftfield, J., Hocking, E.
 P., Schnetger, B., Pearson, E. J., Juggins, S., Fretwell, P., Ireland, L., Ochyra, R., Haworth, A. R., Allen, C. S., Moreton, S.
 G., Davies, S. J., Brumsack, H.-J., Bentley, M. J., and Hodgson, D. A.: Past penguin colony responses to explosive volcanism on the Antarctic Peninsula, Nature Communications, 8, 14914, https://doi.org/10.1038/ncomms14914, 2017.
- Rontani, J.-F. and Volkman, J. K.: Phytol degradation products as biogeochemical tracers in aquatic environments, Organic Geochemistry, 34, 1–35, https://doi.org/10.1016/S0146-6380(02)00185-7, 2003.
- Sargent, J. R. and Falk-Petersen, S.: Ecological investigations on the zooplankton community in balsfjorden, northern Norway: Lipids and fatty acids in *Meganyctiphanes norvegica*, *Thysanoessa raschi* and *T. inermis* during mid-winter, Mar. Biol., 62, 131–137, https://doi.org/10.1007/BF00388175, 1981.
- Sarmiento, J. L., Gruber, N., Brzezinski, M. A., and Dunne, J. P.: High-latitude controls of thermocline nutrients and low latitude biological productivity, Nature, 427, 56–60, https://doi.org/10.1038/nature02127, 2004.
- Shatova, O., Wing, S. R., Gault-Ringold, M., Wing, L., and Hoffmann, L. J.: Seabird guano enhances phytoplankton production in the Southern Ocean, Journal of

- Experimental Marine Biology and Ecology, 483, 74–87, https://doi.org/10.1016/j.jembe.2016.07.004, 2016.
- Shatova, O. A., Wing, S. R., Hoffmann, L. J., Wing, L. C., and Gault-Ringold, M.: Phytoplankton community structure is influenced by seabird guano enrichment in the Southern Ocean, Estuarine Coastal and Shelf Science, 191, 125–135, https://doi.org/10.1016/j.ecss.2017.04.021, 2017.
- Smith, J. A., Hillenbrand, C.-D., Pudsey, C. J., Allen, C. S., and Graham, A. G. C.: The presence of polynyas in the Weddell Sea during the Last Glacial Period with implications for the reconstruction of sea-ice limits and ice sheet history, Earth and Planetary Science Letters, 296, 287–298, https://doi.org/10.1016/j.epsl.2010.05.008, 2010.
- Sparaventi, E., Rodríguez-Romero, A., Barbosa, A., Ramajo, L., and Tovar-Sánchez, A.: Trace elements in Antarctic penguins and the potential role of guano as source of recycled metals in the Southern Ocean, Chemosphere, 285, 131423, https://doi.org/10.1016/j.chemosphere.2021.131423, 2021.
- St John Glew, K., Espinasse, B., Hunt, B. P. V., Pakhomov, E. A., Bury, S. J., Pinkerton, M., Nodder, S. D., Gutiérrez-Rodríguez, A., Safi, K., Brown, J. C. S., Graham, L., Dunbar, R. B., Mucciarone, D. A., Magozzi, S., Somes, C., and Trueman, C. N.: Isoscape Models of the Southern Ocean: Predicting Spatial and Temporal Variability in Carbon and Nitrogen Isotope Compositions of Particulate Organic Matter, Global Biogeochemical Cycles, 35, e2020GB006901, https://doi.org/10.1029/2020GB006901, 2021.
- Stefanova, M. and Disnar, J. R.: Composition and early diagenesis of fatty acids in lacustrine sediments, lake Aydat (France), Organic Geochemistry, 31, 41–55, https://doi.org/10.1016/S0146-6380(99)00134-5, 2000.
- Stevenson, M. A., Hodgson, D. A., Bentley, M. J., Gröcke, D. R., Tunstall, N., Longley, C., Graham, A., and McClymont, E. L: Mid-Holocene sea-ice dynamics and climate in the north-eastern Weddell Sea inferred from an Antarctic snow petrel stomach oil deposit, PANGAEA [dataset bundled publication], https://doi.org/10.1594/PANGAEA.980519, 2025.
- Studer, A. S., Sigman, D. M., Martínez-García, A., Thöle, L. M., Michel, E., Jaccard, S. L., Lippold, J. A., Mazaud, A., Wang, X. T., Robinson, L. F., Adkins, J. F., and Haug, G. H.: Increased nutrient supply to the Southern Ocean during the Holocene and its implications for the pre-industrial atmospheric CO₂ rise, Nature Geoscience, 11, 756–760, https://doi.org/10.1038/s41561-018-0191-8, 2018.
- Sun, L., Xie, Z., and Zhao, J.: A 3,000-year record of penguin populations, Nature, 407, 858–858, https://doi.org/10.1038/35038163, 2000.
- Tatur, A., Myrcha, A., and Niegodzisz, J.: Formation of abandoned penguin rookery ecosystems in the maritime Antarctic, Polar Biology, 17, 405–417, https://doi.org/10.1007/s003000050135, 1997.
- Taylor, F., Whitehead, J., and Domack, E.: Holocene paleoclimate change in the Antarctic Peninsula: evidence from the diatom, sedimentary and geochemical record, Mar. Micropaleontol., 41, 25–43, https://doi.org/10.1016/S0377-8398(00)00049-9, 2001.
- Ter Braak, C. J. F. and Šmilauer, P.: CANOCO Reference manual and CanoDraw for Windows User's guide: Software for Canonical Community Ordination (version 4.5), Microcomputer Power, 2002.

- Totten, R. L., Anderson, J. B., Fernandez, R., and Wellner, J. S.: Marine record of Holocene climate, ocean, and cryosphere interactions: Herbert Sound, James Ross Island, Antarctica, Quaternary Science Reviews, 129, 239–259, https://doi.org/10.1016/j.quascirev.2015.09.009, 2015.
- Turner, J., Guarino, M. V., Arnatt, J., Jena, B., Marshall, G. J., Phillips, T., Bajish, C. C., Clem, K., Wang, Z., Andersson, T., Murphy, E. J., and Cavanagh, R.: Recent Decrease of Summer Sea Ice in the Weddell Sea, Antarctica, Geophysical Research Letters, 47, e2020GL087127, https://doi.org/10.1029/2020GL087127, 2020.
- Valenzuela, L. O., Rowntree, V. J., Sironi, M., and Seger, J.: Stable isotopes (δ^{15} N, δ^{13} C, δ^{34} S) in skin reveal diverse food sources used by southern right whales Eubalaena australis, Marine Ecology Progress Series, 603, 243–255, 2018.
- van den Berg, G. L., Vermeulen, E., Valenzuela, L. O., Bérubé, M., Ganswindt, A., Gröcke, D. R., Hall, G., Hulva, P., Neveceralova, P., Palsbøll, P. J., and Carroll, E. L.: Decadal shift in foraging strategy of a migratory southern ocean predator, Global Change Biology, 27, 1052–1067, https://doi.org/10.1111/gcb.15465, 2021.
- Verleyen, E., Hodgson, D. A., Sabbe, K., Cremer, H., Emslie, S. D., Gibson, J., Hall, B., Imura, S., Kudoh, S., Marshall, G. J., McMinn, A., Melles, M., Newman, L., Roberts, D., Roberts, S. J., Singh, S. M., Sterken, M., Tavernier, I., Verkulich, S., de Vyver, E. V., Van Nieuwenhuyze, W., Wagner, B., and Vyverman, W.: Post-glacial regional climate variability along the East Antarctic coastal margin Evidence from shallow marine and coastal terrestrial records, Earth-Sci. Rev., 104, 199–212, https://doi.org/10.1016/j.earscirev.2010.10.006, 2011.
- Vernet, M., Geibert, W., Hoppema, M., Brown, P. J., Haas, C., Hellmer, H. H., Jokat, W., Jullion, L., Mazloff, M., Bakker, D. C. E., Brearley, J. A., Croot, P., Hattermann, T., Hauck, J., Hillenbrand, C.-D., Hoppe, C. J. M., Huhn, O., Koch, B. P., Lechtenfeld, O. J., Meredith, M. P., Naveira Garabato, A. C., Nöthig, E.-M., Peeken, I., Rutgers van der Loeff, M. M., Schmidtko, S., Schröder, M., Strass, V. H., Torres-Valdés, S., and Verdy, A.: The Weddell Gyre, Southern Ocean: Present Knowledge and Future Challenges, Reviews of Geophysics, 57, 623–708, https://doi.org/10.1029/2018RG000604, 2019.
- Vorrath, M. E., Müller, J., Cárdenas, P., Opel, T., Mieruch, S., Esper, O., Lembke-Jene, L., Etourneau, J., Vieth-Hillebrand, A., Lahajnar, N., Lange, C. B., Leventer, A., Evangelinos, D., Escutia, C., and Mollenhauer, G.: Deglacial and Holocene sea-ice and climate dynamics in the Bransfield Strait, northern Antarctic Peninsula, Clim. Past, 19, 1061–1079, https://doi.org/10.5194/cp-19-1061-2023, 2023.

- Wainright, S. C., Haney, J. C., Kerr, C., Golovkin, A. N., and Flint, M. V.: Utilization of nitrogen derived from seabird guano by terrestrial and marine plants at St. Paul, Pribilof Islands, Bering Sea, Alaska, Marine Biology, 131, 63–71, https://doi.org/10.1007/s002270050297, 1998.
- Wakefield, E. D., McClymont, E. L., Descamps, S., Grecian, W. J., Honan, E. M., Rix, A. S., Robert, H., Sandøy Bråthen, V., and Phillips, R. A.: Variability in foraging ranges of snow petrels and implications for breeding distribution and use of stomach-oil deposits as proxies for paleoclimate, bioRxiv [preprint], 2025.2006.2006.658237, https://doi.org/10.1101/2025.06.06.658237, 8 June 2025.
- Wang, J., Massonnet, F., Goosse, H., Luo, H., Barthélemy, A., and Yang, Q.: Synergistic atmosphere-ocean-ice influences have driven the 2023 all-time Antarctic sea-ice record low, Communications Earth & Environment, 5, 415, https://doi.org/10.1038/s43247-024-01523-3, 2024.
- Warham, J., Watts, R., and Dainty, R. J.: The composition, energy content and function of the stomach oils of petrels (order, procellariiformes), Journal of Experimental Marine Biology and Ecology, 23, 1–13, https://doi.org/10.1016/0022-0981(76)90081-2, 1976.
- Watts, R. and Warham, J.: Structure of some intact lipids of petrel stomach oils, Lipids, 11, 423–429, https://doi.org/10.1007/BF02532831, 1976.
- Wickham, H., Averick, M., Bryan, J., Chang, W., McGowan, L. D. A., François, R., Grolemund, G., Hayes, A., Henry, L., and Hester, J.: Welcome to the Tidyverse, Journal of Open Source Software, 4, 1686, 2019.
- Xavier, J. C., Raymond, B., Jones, D. C., and Griffiths, H.: Biogeography of Cephalopods in the Southern Ocean Using Habitat Suitability Prediction Models, Ecosystems, 19, 220–247, https://doi.org/10.1007/s10021-015-9926-1, 2016.
- Xiao, W., Esper, O., and Gersonde, R.: Last Glacial Holocene climate variability in the Atlantic sector of the Southern Ocean, Quaternary Science Reviews, 135, 115–137, https://doi.org/10.1016/j.quascirev.2016.01.023, 2016.